Modulating Charge Separation and Charge Recombination Dynamics in Porphyrin−Fullerene Linked Dyads and Triads: Marcus-Normal versus Inverted Region

Hiroshi Imahori,*,⊥ Koichi Tamaki,‡ Dirk M. Guldi,*,† Chuping Luo,† Mamoru Fujitsuka,§ Osamu Ito,*,§ Yoshiteru Sakata,‡ and Shunichi Fukuzumi*,⊥

Contribution from the Department of Material and Life Science, Graduate School of Engineering, Osaka University, CREST, Japan Science and Technology Corporation, Suita, Osaka 565-0871, Japan, The Institute of Scientific and Industrial Research, Osaka University, 8-1 Mihoga-oka, Ibaraki, Osaka 567-0047, Japan, Radiation Laboratory, University of Notre Dame, Notre Dame, Indiana 46556, and Institute for Chemical Reaction Science, Tohoku University, Katahira, Aoba-ku, Sendai 980-8577, Japan

Received September 11, 2000. Revised Manuscript Received January 2, 2001

Abstract: Photoinduced charge separation (CS) and charge recombination (CR) processes have been examined in various porphyrin−fullerene linked systems (i.e., dyads and triads) by means of time-resolved transient absorption spectroscopy and fluorescence lifetime measurements. The investigated compounds comprise a homologous series of rigidly linked, linear donor−acceptor arrays with different donor−acceptor separations and diversified donor strength: freebase porphyrin−C_{60} dyad (**H_2P-C_{60}**), zincporphyrin−C_{60} dyad (**ZnP-C_{60}**), ferrocene−zincporphyrin−C_{60} triad (**Fc-ZnP-C_{60}**), ferrocene−freebase porphyrin−C_{60} triad (**Fc-H_2P-C_{60}**), and zincporphyrin−freebase porphyrin−C_{60} triad (**ZnP-H_2P-C_{60}**). Most importantly, the lowest lying charge-separated state of all the investigated systems, namely, that of ferrocenium ion (Fc^+) and the C_{60} radical anion ($C_{60}^{\bullet-}$) pair in the **Fc-ZnP-C_{60}** triad, has been generated with the highest quantum yields (close to unity) and reveals a lifetime as long as 16 μs. Determination of CS and CR rate constants, together with the one-electron redox potentials of the donor and acceptor moieties in different solvents, has allowed us to examine the driving force dependence ($-\Delta G^0_{ET}$) of the electron-transfer rate constants (k_{ET}). Hereby, the semilogarithmic plots (i.e., log k_{ET} versus $-\Delta G^0_{ET}$) lead to the evaluation of the reorganization energy (λ) and the electronic coupling matrix element (V) in light of the Marcus theory of electron-transfer reactions: $\lambda = 0.66$ eV and $V = 3.9$ cm^{-1} for **ZnP-C_{60}** dyad and $\lambda = 1.09$ eV and $V = 0.019$ cm^{-1} for **Fc-ZnP-C_{60}**, **Fc-H_2P-C_{60}**, and **ZnP-H_2P-C_{60}** triads. Interestingly, the Marcus plot in **Fc-ZnP-C_{60}**, **Fc-H_2P-C_{60}**, and **ZnP-H_2P-C_{60}** has provided clear evidence for intramolecular CR located in both the normal and inverted regions of the Marcus parabola. The coefficient for the distance dependence of V (damping factor: $\beta_{CR} = 0.58$ Å^{-1}) is deduced which depends primarily on the nature of the bridging molecule.

Introduction

The primary challenge in artificial photosynthesis lies in the design of photoinduced electron transfer (ET) systems, which, upon photoexcitation, give rise to a long-lived charge-separated state in high quantum yields. An important design consideration merging from the natural process is that photosynthesis utilizes relays of multistep ETs, which facilitate separating radical ion pairs over long distances and, thereby, successfully retarding energy-wasting charge recombination (CR).

Along this line considerable efforts have been directed toward the preparation of novel donor−acceptor systems with the purpose being to prolong the lifetime of the charge-separated state, while, simultaneously, optimizing the efficiency of charge separation (CS).[1−6] Despite the extreme difficulties, connected with the design and synthesis of rigidly spaced ensembles, a long-distance CS can only be attained in multistep ET systems. In particular, in triad, tetrad, and pentad structures distantly

* Address correspondence to these authors. E-mail: imahori@ap.chem.eng.osaka-u.ac.jp; guldi.1@nd.edu; ito@icrs.tohoku.ac.jp; fukuzumi@ap.chem.eng.osaka-u.ac.jp.

⊥ Department of Material and Life Science, Graduate School of Engineering, Osaka University.

‡ The Institute of Scientific and Industrial Research, Osaka University.

† Radiation Laboratory, University of Notre Dame.

§ Institute for Chemical Reaction Science, Tohoku University.

(1) (a) Connolly, J. S.; Bolton, J. R. In *Photoinduced Electron Transfer*; Fox, M. A., Chanon, M., Eds.; Elsevier: Amsterdam, 1988; Part D, pp 303−393. (b) Wasielewski, M. R. In *Photoinduced Electron Transfer*; Fox, M. A., Chanon, M., Eds.; Elsevier: Amsterdam, 1988; Part A, pp 161−206. (c) Meyer, T. J. *Acc. Chem. Res.* **1989**, *22*, 163. (d) Bard, A. J.; Fox, M. A. *Acc. Chem. Res.* **1995**, *28*, 141.

(2) (a) Wasielewski, M. R. *Chem. Rev.* **1992**, *92*, 435. (b) Gust, D.; Moore, T. A.; Moore, A. L. *Acc. Chem. Res.* **1993**, *26*, 198. (c) Gust, D.; Moore, T. A. In *The Porphyrin Handbook*; Kadish, K. M., Smith, K. M., Guilard, R., Eds.; Academic Press: San Diego, CA, 2000; Vol. 8, pp 153−190. (d) Gust, D.; Moore, T. A.; Moore, A. L. *Pure Appl. Chem.* **1998**, *70*, 2189.

(3) (a) Oevering, H.; Paddon-Row, M. N.; Heppener, M.; Oliver, A. M.; Cotsaris, E.; Verhoeven, J. W.; Hush, N. S. *J. Am. Chem. Soc.* **1987**, *109*, 3258. (b) Paddon-Row, M. N. *Acc. Chem. Res.* **1994**, *27*, 18. (c) Verhoeven, J. W. In *Electron Transfer*; Jortner, J., Bixon, M., Eds.; John Wiley & Sons: New York, 1999; Part 1, pp 603−644. (d) Jordan, K. D.; Paddon-Row, M. N. *Chem. Rev.* **1992**, *92*, 395.

(4) (a) Chambron, J.-C.; Chardon-Noblat, S.; Harriman, A.; Heitz, V.; Sauvage, J.-P. *Pure Appl. Chem.* **1993**, *65*, 2343. (b) Harriman, A.; Sauvage, J.-P. *Chem. Soc. Rev.* **1996**, *26*, 41. (c) Blanco, M.-J.; Jiménez, M. C.; Chambron, J.-C.; Heitz, V.; Linke, M.; Sauvage, J.-P. *Chem. Soc. Rev.* **1999**, *28*, 293. (d) Kurreck, H.; Huber, M. *Angew. Chem. Int. Ed. Engl.* **1995**, *34*, 849. (e) Balzani, V.; Juris, A.; Venturi, M.; Campagna, S.; Serroni, S. *Chem. Rev.* **1996**, *96*, 759. (f) Amabilino, D. B.; Stoddart, J. F. *Chem. Rev.* **1995**, *95*, 2725.

10.1021/ja003346i CCC: $20.00
Published on Web 02/23/2001

separated donor−acceptor radical ion pairs are generated as a result of an initial CS followed, in succession, by several charge shift (CSH) reactions along well-tuned redox gradients.

In this context, an intrinsic property of the 3-dimensional electron acceptor C_{60}, namely, its small reorganization energy (λ) associated with ET reactions, evokes a number of important consequences.[6−8] Most importantly, CS and CR processes are accelerated and decelerated, respectively, relative to comparable systems in which, however, 2-dimensional acceptor moieties are used (i.e., *p*-benzoquinone). Therefore, efficient stepwise CS in a fullerene-containing triad, along a well-designed redox gradient, can be realized regardless of the solvent environment, whereas this takes place only occasionally in conventional systems.[1−6] It should be mentioned that these effects are the small reorganization energy and its consequences resulting from the fullerene's unique structure and symmetry, which are ultimately responsible for its high degree of its delocalization and structural rigidity.[6−8]

The Marcus theory of ET provides a valuable guide for controlling and optimizing the efficiency of CS versus CR. In particular, the rates of CR can be markedly slowed by shifting them deep into the inverted region of the Marcus parabola, where the driving force ($-\Delta G^0_{ET}$) is larger than the total reorganization energy (λ) of ET.[9,10] Extensive efforts have been directed toward establishing the driving force dependence of the ET rates,[11−17] and thereby probing the inverted region of the Marcus curve in donor−acceptor couples.[8a,11b,12−15] As pointed out recently by Mataga,[11b] however, the bell-shaped driving force dependence of the intramolecular CR rates including both the normal and inverted regions for donor−acceptor linked systems has yet to be demonstrated.

For intermolecular ET dynamics, the inverted region has rarely been observed.[8a,11b,14,15] This infrequent manifestation has been rationalized in terms of the distribution of donor−acceptor distance on the energy gap.[11b] In particular, enlarging the driving force, especially into the highly exergonic region ($-\Delta G^0_{ET} \gg 0$), results in an increase in λ, especially in the solvent reorganization energy (λ_s). It should be emphasized that this, in turn, governs the high CS rates.[9] In addition, the Marcus theory hypothesizes that λ_s also increases with intermolecular donor−acceptor distance.[9] Taking these two effects into account it seems plausible that observation of the inverted region in intermolecular ET systems is extremely difficult.[11b] Such a change in λ, as a function of separation distance, awaits experimental confirmation. An appealing approach for accomplishing this would be to determine λ values, associated with special sets of molecules assembled so that each set would consist of an identical homologous series of donor−acceptor pairs but with each set having a different characteristic intramolecular donor−acceptor separation. Such an experimental strategy for the evaluation of ET parameters at different donor−acceptor separations necessitates the design of a minimum of two homologous donor−acceptor linked series (i.e., dyads and triads). In these ensembles the redox potentials of donor−acceptor moieties should be changed without affecting the relative distance.

In the present study a novel family of dyad and triad systems was designed by combining the following building blocks (electron donor) in various orders: H_2P (P = tetraphenylporphyrin dianion), ZnP, and ferrocene (Fc) with the electron accepting C_{60} (see Figure 1). Thus, the above criteria, namely, different donor−acceptor separations and/or different donor strengths, are unequivocally given to probe the reorganization energies and the electronic coupling matrix elements in fullerene-containing ensembles. We report herein the intramolecular CR processes in both the normal and inverted regions of the Marcus curve, using a series of ferrocene−porphyrin−fullerene triads **Fc-ZnP-C$_{60}$**[18−20] and **Fc-H$_2$P-C$_{60}$**,[19] and zincporphyrin−free-base porphyrin−fullerene triad **ZnP-H$_2$P-C$_{60}$**[21] (Figure 1) with equal edge-to-edge distances (R_{ee}) of 30.3 Å. In addition, these triads will be compared to a zincporphyrin−fullerene dyad **ZnP-C$_{60}$** (R_{ee} = 11.9 Å).[21−23] Hereby, we highlight the immediate impact on the reorganization energy and the electronic coupling matrix element that stem from fine-tuning the nature and the separation distance of the intervening spacer. In sum, the present study provides an unambiguous dependence of ET rate constants on both the distance and driving force in a series of homologous donor−acceptor arrays.

(5) (a) Osuka, A.; Mataga, N.; Okada, T. *Pure Appl. Chem.* **1997**, *69*, 797. (b) Maruyama, K.; Osuka, A.; Mataga, N. *Pure Appl. Chem.* **1994**, *66*, 867. (c) Piotrowiak, P. *Chem. Soc. Rev.* **1999**, *28*, 143.

(6) (a) Imahori, H.; Sakata, Y. *Adv. Mater.* **1997**, *9*, 537. (b) Imahori, H.; Sakata, Y. *Eur. J. Org. Chem.* **1999**, 2445. (c) Guldi, D. M. *Chem. Commun.* **2000**, 321. (d) Guldi, D. M.; Prato, M. *Acc. Chem. Res.* **2000**, *33*, 695. (e) Fukuzumi, S.; Imahori, H. In *Electron Transfer in Chemistry*; Balzani, V., Ed.; Wiley-VCH: Weinheim, 2000, in press.

(7) (a) Imahori, H.; Hagiwara, K.; Akiyama, T.; Aoki, M.; Taniguchi, S.; Okada, T.; Shirakawa, M.; Sakata, Y. *Chem. Phys. Lett.* **1996**, *263*, 545. (b) Tkachenko, N. V.; Guenther, C.; Imahori, H.; Tamaki, K.; Sakata, Y.; Fukuzumi, S.; Lemmetyinen, H. *Chem. Phys. Lett.* **2000**, *326*, 344. (c) Imahori, H.; Tkachenko, N. V.; Vehmanen, V.; Tamaki, K.; Lemmetyinen, H.; Sakata, Y.; Fukuzumi, S. *J. Phys. Chem. A* **2001**, *105*, 1750.

(8) (a) Guldi, D. M.; Asmus, K.-D. *J. Am. Chem. Soc.* **1997**, *119*, 5744. (b) Guldi, D. M.; Neta, P.; Asmus, K.-D. *J. Phys. Chem.* **1994**, *98*, 4617.

(9) (a) Marcus, R. A. *Annu. Rev. Phys. Chem.* **1964**, *15*, 155. (b) Marcus, R. A.; Sutin, N. *Biochim. Biophys. Acta* **1985**, *811*, 265. (c) Marcus, R. A. *Angew. Chem. Int. Ed. Engl.* **1993**, *32*, 1111.

(10) (a) Bixon, M.; Jortner, J. In *Electron Transfer*; Jortner, J., Bixon, M., Eds.; John Wiley & Sons: New York, 1999; Part 1, pp 35−202. (b) Ulstrup, J.; Jortner, J. *J. Chem. Phys.* **1975**, *63*, 4358.

(11) (a) Rehm, D.; Weller, A. *Isr. J. Chem.* **1970**, *7*, 259. (b) Mataga, N.; Miyasaka, H. In *Electron Transfer*; Jortner, J., Bixon, M., Eds.; John Wiley & Sons: New York, 1999; Part 2, pp 431−496.

(12) (a) Miller, J. R.; Calcaterra, L. T.; Closs, G. L. *J. Am. Chem. Soc.* **1984**, *106*, 3047. (b) Closs, G. L.; Miller, J. R. *Science* **1988**, *240*, 440.

(13) Wasielewski, M. R.; Niemczyk, M. P.; Svec, W. A.; Pewitt, E. B. *J. Am. Chem. Soc.* **1985**, *107*, 1080.

(14) (a) Gould, I. R.; Moody, R.; Farid, S. *J. Am. Chem. Soc.* **1988**, *110*, 7242. (b) Gould, I. R.; Farid, S. *Acc. Chem. Res.* **1996**, *29*, 522.

(15) (a) Mataga, N.; Kanda, Y.; Okada, Y. *J. Phys. Chem.* **1986**, *90*, 3880. (b) Asahi, T.; Mataga, N. *J. Phys. Chem.* **1991**, *95*, 1956.

(16) (a) Harrison, R. J.; Pearce, B.; Beddard, G. S.; Cowan, J. A.; Sanders, J. K. M. *Chem. Phys.* **1987**, *116*, 429. (b) Asahi, T.; Ohkohchi, M.; Matsusaka, R.; Mataga, N.; Zhang, R. P.; Osuka, A.; Maruyama, K. *J. Am. Chem. Soc.* **1993**, *115*, 5665. (c) Harriman, A.; Heitz, V.; Sauvage, J.-P. *J. Phys. Chem.* **1993**, *97*, 5940. (d) Khundkar, L. R.; Perry, J. W.; Hanson, J. E.; Dervan, P. B. *J. Am. Chem. Soc.* **1994**, *116*, 9700. (e) Heitele, H.; Pöllinger, F.; Häberle, T.; Michel-Beyerle, M. E.; Staab, H. A. *J. Phys. Chem.* **1994**, *98*, 7402. (f) Macpherson, A. N.; Liddell, P. A.; Lin, S.; Noss, L.; Seely, G. R.; DeGraziano, J. M.; Moore, A. L.; Moore, T. A.; Gust, D. *J. Am. Chem. Soc.* **1995**, *117*, 7202. (g) Häberle, T.; Hirsch, J.; Pöllinger, F.; Heitele, H.; Michel-Beyerle, M. E.; Ander, C.; Döhling, A.; Krieger, C.; Rückemann, A.; Staab, H. A. *J. Phys. Chem.* **1996**, *100*, 18269. (h) Tsue, H.; Imahori, H.; Kaneda, T.; Tanaka, Y.; Okada, T.; Tamaki, K.; Sakata, Y. *J. Am. Chem. Soc.* **2000**, *122*, 2279.

(17) (a) DeGraziano, J. M.; Liddell, P. A.; Leggett, L.; Moore, A. L.; Moore, T. A.; Gust, D. *J. Phys. Chem.* **1994**, *98*, 1758. (b) Osuka, A.; Noya, G.; Taniguchi, S.; Okada, T.; Nishimura, Y.; Yamazaki, I.; Mataga, N. *Chem. Eur. J.* **2000**, *6*, 33.

(18) Fujitsuka, M.; Ito, O.; Imahori, H.; Yamada, K.; Yamada, H.; Sakata, Y. *Chem. Lett.* **1999**, 721.

(19) Imahori, H.; Yamada, H.; Nishimura, Y.; Yamazaki, I.; Sakata, Y. *J. Phys. Chem. B* **2000**, *104*, 2099.

(20) Imahori, H.; Tamaki, K.; Yamada, H.; Yamada, K.; Sakata, Y.; Nishimura, Y.; Yamazaki, I.; Fujitsuka, M.; Ito, O. *Carbon* **2000**, *38*, 1599.

(21) Luo, C.; Guldi, D. M.; Imahori, H.; Tamaki, K.; Sakata, Y. *J. Am. Chem. Soc.* **2000**, *122*, 6535.

(22) Yamada, K.; Imahori, H.; Nishimura, Y.; Yamazaki, I.; Sakata, Y. *Chem. Lett.* **1999**, 895.

(23) Imahori, H.; El-Khouly, M. E.; Fujitsuka, M.; Ito, O.; Sakata, Y.; Fukuzumi, S. *J. Phys. Chem. A.* **2001**, *105*, 325.

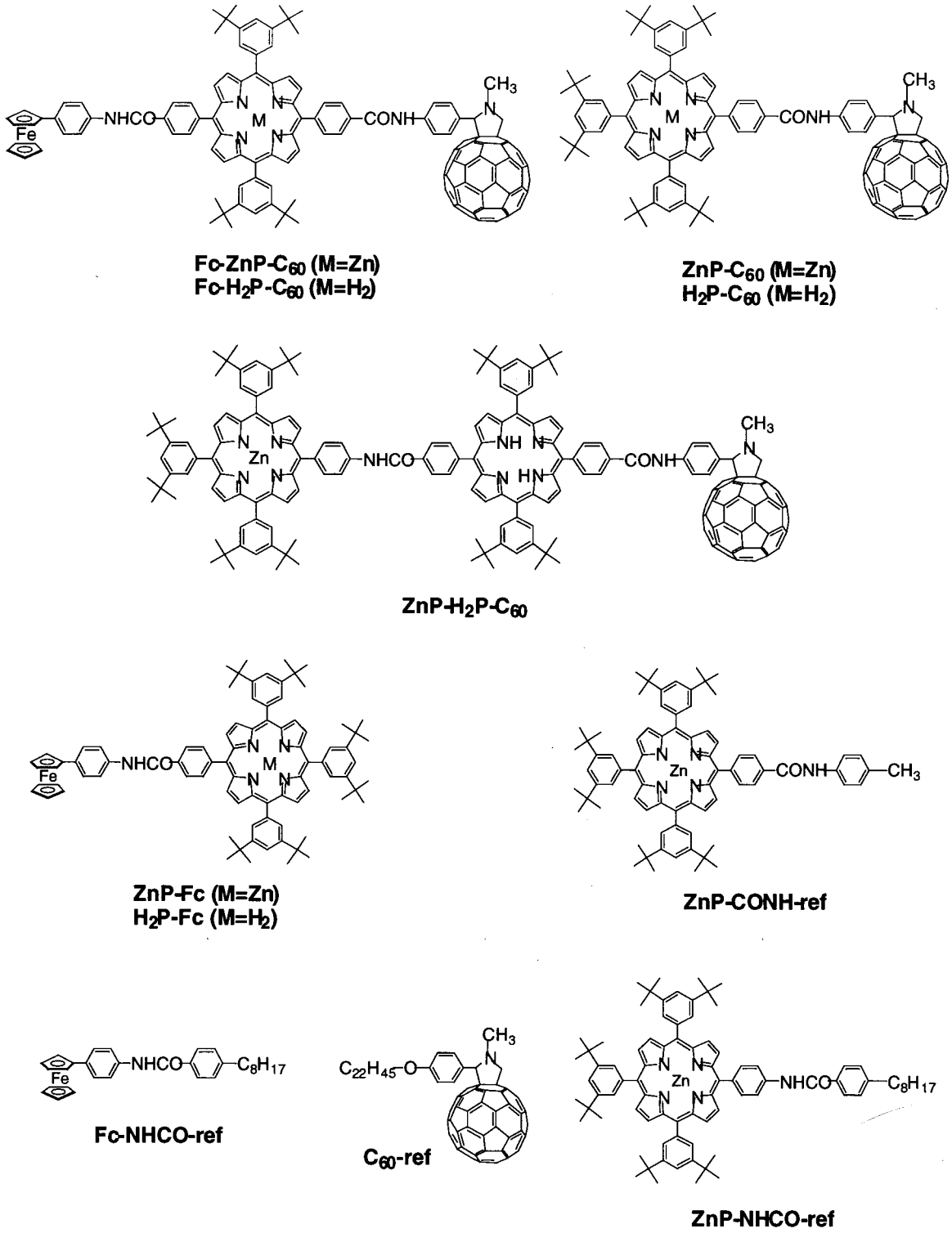

Figure 1. Structures of molecular triads, dyads, and references used in this study.

Results and Discussion

Synthesis and Characterization. The synthesis and characterization of all the compounds (**Fc-ZnP-C_{60}**, **Fc-H_2P-C_{60}**, **ZnP-C_{60}**, **H_2P-C_{60}**, **ZnP-H_2P-C_{60}**, **ZnP-Fc**, **H_2P-Fc**, **ZnP-CONH-ref**, **ZnP-NHCO-ref**, **Fc-NHCO-ref**, and **C_{60}-ref** (Figure 1)) are described in details in the Supporting Information (pp S1−S7). It is important to note that the absorption spectra of **Fc-ZnP-C_{60}**, **Fc-H_2P-C_{60}**, **ZnP-C_{60}**, **H_2P-C_{60}**, and **ZnP-H_2P-C_{60}** in benzonitrile are reasonable superpositions of the spectra of component chromophores making up these molecules. This supports the notion that there is a lack of electronic interaction, long- or short-range, between the individual chromophores in their ground state configuration. Principally similar superpositions of component spectra were found in THF and DMF solutions.

One-Electron Redox Potentials and ET Driving Force. An accurate determination of the driving force ($-\Delta G^0_{ET}$) for all the intramolecular ET processes required measuring the redox potentials of the reference chromophores (**ZnP-CONH-ref**,

Table 1. One-Electron Redox Potentials (E^0) of Porphyrin, Ferrocene, and C_{60} References in Various Solvents (vs Fc/Fc^+)[a]

	THF ($\epsilon_s = 7.58$)		benzonitrile ($\epsilon_s = 25.2$)		DMF ($\epsilon_s = 36.7$)	
compd	E^0_{ox}/V	E^0_{red}/V	E^0_{ox}/V	E^0_{red}/V	E^0_{ox}/V	E^0_{red}/V
ZnP-CONH-ref	0.40	−1.96	0.34	−1.82	0.29	−1.80
	0.73		0.71		0.55	
ZnP-NHCO-ref	0.35	*b*	0.30	−1.85	0.25	−1.84
	0.69		0.67		0.51	
Fc-NHCO-ref	−0.02		−0.01		−0.01	
C_{60}-ref		−1.02		−1.04		−0.92
		−1.57		−1.45		−1.38

[a] The redox potentials were measured by differential pulse voltammetry in THF, benzonitrile, and DMF with 0.1 M *n*-Bu_4NPF_6 as a supporting electrolyte with a sweep rate of 10 mV s^{-1}. [b] Not detectable within a sweep range of 0 to −2.0 V.

ZnP-NHCO-ref, **Fc-NHCO-ref**, and **C_{60}-ref**) in various solvents. The differential pulse voltammetry was performed in THF, benzonitrile, and DMF solutions containing the same supporting electrolyte (i.e., 0.1 M *n*-Bu_4NPF_6). For example, the peak positions of **ZnP-NHCO-ref** (see Supporting Information (p S10)), which correspond to the first and the second reversible oxidation of the porphyrin moiety, shift progressively to a more negative direction as the solvent polarity indicated by the dielectric constant (ϵ_s) was changed in the following order: THF ($\epsilon_s = 7.58$) < benzonitrile ($\epsilon_s = 25.2$) < DMF ($\epsilon_s = 36.7$) (Table 1). Negative shifts in the oxidation potentials in increasingly more polar solvents are principally rationalized by a stronger solvation, which the resulting radical cations and dications of the porphyrin moieties experience. Similar negative shifts were noted for the first and second oxidation steps in **ZnP-CONH-ref** (Table 1). On the contrary, the first one-electron oxidation potential of **Fc-NHCO-ref** remains nearly constant, despite the substantial increase in solvent polarity. The last reference (i.e., **C_{60}-ref**) exhibits positive shifts for the underlying first and second one-electron reduction potentials, which are parallel to the preferential stabilization of the electron relative to the radical anion with the increase in solvent polarity. Table 1 summarizes all the redox potentials of the investigated references.

The driving forces ($-\Delta G^0_{ET(CR)}$ in eV) for the intramolecular CR processes from C_{60} radical anion ($C_{60}^{\bullet-}$) to zincporphyrin radical cation ($ZnP^{\bullet+}$) or ferricenium ion (Fc^+) in **$ZnP^{\bullet+}$-$C_{60}^{\bullet-}$**, **Fc^+-ZnP-$C_{60}^{\bullet-}$**, **Fc^+-H_2P-$C_{60}^{\bullet-}$**, and **$ZnP^{\bullet+}$-H_2P-$C_{60}^{\bullet-}$** were calculated by eq 1, where *e* stands for the elementary charge.

$$-\Delta G^0_{ET(CR)} = e[E^0_{ox}(D^{\bullet+}/D) - E^0_{red}(A/A^{\bullet-})] \qquad (1)$$

In short, $[E^0_{ox}(D^{\bullet+}/D)]$ is the first one-electron oxidation potential of the donor (zincporphyrin or ferrocene) moiety, while $[E^0_{red}(A/A^{\bullet-})]$ refers to the first one-electron reduction potential of the acceptor (C_{60}) moiety in THF, benzonitrile, and DMF. The accordingly calculated $-\Delta G^0_{ET(CR)}$ values are listed in Tables 2−4. Furthermore, the driving forces ($-\Delta G^0_{ET(CS)}$ in eV) for the intramolecular CS processes (**ZnP-C_{60}**, **Fc-ZnP-C_{60}**, **Fc-H_2P-C_{60}**, and **ZnP-H_2P-C_{60}**) were determined by:

$$-\Delta G^0_{ET(CS)} = \Delta E_{0-0} + \Delta G^0_{ET(CR)} \qquad (2)$$

Hereby, ΔE_{0-0} is the energy of the 0−0 transition energy gap between the lowest excited state and the ground state. The $-\Delta G^0_{ET(CS)}$ values are given in Tables 2−4. It should be noted that the Coulombic terms in the present donor−acceptor systems are negligible, especially in solvents with moderate or high polarity, because of the relatively large R_{ee} values (>11 Å) employed.[18−23]

Photodynamics of Porphyrin−Fullerene Linked Systems. Time-resolved transient absorption spectra, following picosecond and nanosecond laser pulses, were employed to examine the photodynamics of **ZnP-C_{60}**, **H_2P-C_{60}**, **Fc-ZnP-C_{60}**, **Fc-H_2P-C_{60}**, and **ZnP-H_2P-C_{60}**. Concisely, in THF, benzonitrile, and DMF the spectral characteristics of $ZnP^{\bullet+}$ and $C_{60}^{\bullet-}$ were found for the **ZnP-C_{60}** and **ZnP-H_2P-C_{60}** ensembles, while **Fc-ZnP-C_{60}** and **Fc-H_2P-C_{60}** triads gave rise to those of Fc^+ and $C_{60}^{\bullet-}$ (see below).[24−32] To monitor the intramolecular ET dynamics, the absorption of the one-electron reduced form of the electron acceptor ($C_{60}^{\bullet-}$) was analyzed in the near-infrared region (NIR) around 1000 nm.

Photophysics of Porphyrin-Fullerene Linked Dyads. (a) ZnP-C_{60}: Time-resolved transient absorption spectra of **ZnP-C_{60}** were measured by pico- and nanosecond laser photolysis. For instance, picosecond time-resolved absorption spectra, as recorded typically for a benzonitrile solution of **ZnP-C_{60}**

(24) (a) Martín, N.; Sánchez, L.; Illescas, B.; Pérez, I. *Chem. Rev.* **1998**, *98*, 2527. (b) Prato, M. *J. Mater. Chem.* **1997**, *7*, 1097. (c) Diederich, F.; Gómez-López, M. *Chem. Soc. Rev.* **1999**, *28*, 263. (d) Sun, Y.-P.; Riggs, J. E.; Guo, Z.; Rollins, H. W. In *Optical and Electronic Properties of Fullerenes and Fullerene-Based Materials*; Shinar, J., Vardeny, Z. V., Kafafi, Z. H., Eds.; Marcel Dekker: New York, 2000; pp 43−81. (e) Guldi, D. M.; Kamat, P. V. In *Fullerenes*; Kadish, K. M., Ruoff, R. S., Eds.; John Wiley & Sons: New York, 2000; Chapter 5, pp 225−281. (f) Fukuzumi, S.; Guldi, D. M. In *Electron Transfer in Chemistry*; Balzani, V., Ed.; Wiley-VCH: Weinheim, 2001, in press.

(25) (a) Liddell, P. A.; Sumida, J. P.; Macpherson, A. N.; Noss, L.; Seely, G. R.; Clark, K. N.; Moore, A. L.; Moore, T. A.; Gust, D. *Photochem. Photobiol.* **1994**, *60*, 537. (b) Kuciauskas, D.; Lin, S.; Seely, G. R.; Moore, A. L.; Moore, T. A.; Gust, D.; Drovetskaya, T.; Reed, C. A.; Boyd, P. D. W. *J. Phys. Chem.* **1996**, *100*, 15926. (c) Gust, D.; Moore, T. A.; Moore, A. L. *Res. Chem. Intermed.* **1997**, *23*, 621. (d) Liddell, P. A.; Kuciauskas, D.; Sumida, J. P.; Nash, B.; Nguyen, D.; Moore, A. L.; Moore, T. A.; Gust, D. *J. Am. Chem. Soc.* **1997**, *119*, 1400. (e) Carbonera, D.; Di Valentin, M.; Corvaja, C.; Agostini, G.; Giacometti, G.; Liddell, P. A.; Kuciauskas, D.; Moore, A. L.; Moore, T. A.; Gust, D. *J. Am. Chem. Soc.* **1998**, *120*, 4398. (f) Kuciauskas, D.; Liddell, P. A.; Moore, T. A.; Gust, D. *J. Am. Chem. Soc.* **1998**, *120*, 10880. (g) Kuciauskas, D.; Liddell, P. A.; Lin, S.; Johnson, T. E.; Weghorn, S. J.; Lindsey, J. S.; Moore, A. L.; Moore, T. A.; Gust, D. *J. Am. Chem. Soc.* **1999**, *121*, 8604. (h) Kuciauskas, D.; Liddell, P. A.; Lin, S.; Stone, S. G.; Moore, A. L.; Moore, T. A.; Gust, D. *J. Phys. Chem. B* **2000**, *104*, 4307.

(26) (a) Williams, R. M.; Zwier, J. M.; Verhoeven, J. W. *J. Am. Chem. Soc.* **1995**, *117*, 4093. (b) Lawson, J. M.; Oliver, A. M.; Rothenfluh, D. F.; An, Y.-Z.; Ellis, G. A.; Ranasinghe, M. G.; Khan, S. I.; Franz, A. G.; Ganapathi, P. S.; Shephard, M. J.; Paddon-Row, M. N.; Rubin, Y. *J. Org. Chem.* **1996**, *61*, 5032. (c) Williams, R. M.; Koeberg, M.; Lawson, J. M.; An, Y.-Z.; Rubin, Y.; Paddon-Row, M. N.; Verhoeven, J. W. *J. Org. Chem.* **1996**, *61*, 5055. (d) Bell, T. D. M.; Smith, T. A.; Ghiggino, K. P.; Ranasinghe, M. G.; Shephard, M. J.; Paddon-Row, M. N. *Chem. Phys. Lett.* **1997**, *268*, 223.

(27) (a) Jensen, A. W.; Wilson, S. R.; Schuster, D. I. *Bioorg. Med. Chem.* **1996**, *4*, 767. (b) Baran, P. S.; Monaco, R. R.; Khan, A. U.; Schuster, D. I.; Wilson, S. R. *J. Am. Chem. Soc.* **1997**, *119*, 8363. (c) Schuster, D. I.; Cheng, P.; Wilson, S. R.; Prokhorenko, V.; Katterle, M.; Holzwarth, A. R.; Braslavsky, S. E.; Klihm, G.; Williams, R. M.; Luo, C. *J. Am. Chem. Soc.* **1999**, *121*, 11599. (d) Fong, R., II; Schuster, D. I.; Wilson, S. R. *Org. Lett.* **1999**, *1*, 729. (e) Wilson, S. R.; Schuster, D. I.; Nuber, B.; Meier, M. S.; Maggini, M.; Prato, M.; Taylor, R. *Fullerenes*; Kadish, K. M., Ruoff, R. S., Eds.; John Wiley & Sons: New York, 2000; Chapter 3, pp 91−176.

(28) (a) Nierengarten, J.-F.; Schall, C.; Nicoud, J.-F. *Angew. Chem. Int. Ed.* **1998**, *37*, 1934. (b) Bourgeois, J.-P.; Diederlich, F.; Echegoyen, L.; Nierengarten, J.-F. *Helv. Chim. Acta* **1998**, *81*, 1835. (c) Armaroli, N.; Diederlich, F.; Dietrich-Buchecker, C. O.; Flamigni, L.; Marconi, G.; Nierengarten, J.-F.; Sauvage, J.-P. *Chem. Eur. J.* **1998**, *4*, 406. (d) Armspach, D.; Constable, E. C.; Diederlich, F.; Housecroft, C. E.; Nierengarten, J.-F. *Chem. Eur. J.* **1998**, *4*, 723. (e) Camps, X.; Dietel, E.; Hirsch, A.; Pyo, S.; Echegoyen, L.; Hackbarth, S.; Röder, B. *Chem. Eur. J.* **1999**, *5*, 2362. (f) Armaroli, N.; Marconi, G.; Echegoyen, L.; Bourgeois, J.-P.; Diederlich, F. *Chem. Eur. J.* **2000**, *6*, 1629. (g) van Hall, P. A.; Knol, J.; Langeveld-Voss, B. M. W.; Meskers, S. C. J.; Hummelen, J. C.; Janssen, R. A. J. *J. Phys. Chem. A* **2000**, *104*, 5974. (h) Eckert, J.-F.; Nicoud, J.-F.; Nierengarten, J.-F.; Liu, S.-G.; Echegoyen, L.; Barigelletti, F.; Armaroli, N.; Ouali, L.; Krasnikov, V.; Hadziioannou, G. *J. Am. Chem. Soc.* **2000**, *122*, 7467.

Table 2. ET Rate Constants (k_{ET}) for CS and CR and the Driving Force ($-\Delta G^0_{ET}$) in **ZnP-C$_{60}$** and **H$_2$P-C$_{60}$**

solvent	initial state[a]	final state[a]	$-\Delta G^0_{ET}$/eV	k_{ET}/s^{-1},[b]	Φ[c]
THF	^{1}ZnP*-C$_{60}$ (2.07 eV)	ZnP$^{\bullet+}$-C$_{60}^{\bullet-}$ (1.42 eV)	0.65	$k_{ET(CS1)} = 1.3 \times 10^{10}$,[d]	$\Phi_{CS1}(^1\text{ZnP*}) = 0.96$
($\epsilon_s = 7.58$)	ZnP-^{1}C$_{60}$* (1.75 eV)	ZnP$^{\bullet+}$-C$_{60}^{\bullet-}$ (1.42 eV)	0.33	$k_{ET(CS2)} = 5.1 \times 10^8$	$\Phi_{CS2}(^1\text{C}_{60}\text{*}) = 0.40$
	ZnP-^{3}C$_{60}$* (1.50 eV)	ZnP$^{\bullet+}$-C$_{60}^{\bullet-}$ (1.42 eV)	0.08	$k_{ET(CS3)} = 1.6 \times 10^7$	$\Phi_{CS3}(^3\text{C}_{60}\text{*}) \sim 1$
	ZnP$^{\bullet+}$-C$_{60}^{\bullet-}$ (1.42 eV)	ZnP−C$_{60}$	1.42	$k_{ET(CR1)} = 3.7 \times 10^5$	
benzonitrile	^{1}ZnP*-C$_{60}$ (2.04 eV)	ZnP$^{\bullet+}$-C$_{60}^{\bullet-}$ (1.38 eV)	0.66	$k_{ET(CS1)} = 9.5 \times 10^9$	$\Phi_{CS1}(^1\text{ZnP*}) = 0.95$
($\epsilon_s = 25.2$)	ZnP-^{1}C$_{60}$* (1.75 eV)	ZnP$^{\bullet+}$-C$_{60}^{\bullet-}$ (1.38 eV)	0.37	$k_{ET(CS2)} = 5.5 \times 10^8$	$\Phi_{CS2}(^1\text{C}_{60}\text{*}) = 0.42$
	ZnP-^{3}C$_{60}$* (1.50 eV)	ZnP$^{\bullet+}$-C$_{60}^{\bullet-}$ (1.38 eV)	0.12	$k_{ET(CS3)} = 1.5 \times 10^7$	$\Phi_{CS3}(^3\text{C}_{60}\text{*}) \sim 1$
	^{3}ZnP*-C$_{60}$ (1.53 eV)	ZnP$^{\bullet+}$-C$_{60}^{\bullet-}$ (1.38 eV)	0.15	$k_{ET(CS4)} > 1.5 \times 10^7$	$\Phi_{CS4}(^3\text{ZnP*}) \sim 1$
	ZnP$^{\bullet+}$-C$_{60}^{\bullet-}$ (1.38 eV)	ZnP−C$_{60}$	1.38	$k_{ET(CR1)} = 1.3 \times 10^6$,[e]	$\Phi_{CS}(\text{total})$[f] $= 0.85$[e](0.99)
	^{1}H$_2$P*−C$_{60}$ (1.89 eV)	H$_2$P$^{\bullet+}$-C$_{60}^{\bullet-}$ (1.59 eV)	0.30	$k_{ET(CS1)} = 5.2 \times 10^9$,[e]	$\Phi_{CS1}(^1\text{H}_2\text{P*}) = 0.98$[e]
DMF	^{1}ZnP*-C$_{60}$ (2.06 eV)	ZnP$^{\bullet+}$-C$_{60}^{\bullet-}$ (1.21 eV)	0.85	$k_{ET(CS1)} = 1.3 \times 10^{10}$,[d]	$\Phi_{CS1}(^1\text{ZnP*}) = 0.96$
(ϵ_s=36.7)	ZnP$^{\bullet+}$-C$_{60}^{\bullet-}$ (1.21 eV)	ZnP−C$_{60}$	1.21	$k_{ET(CR1)} = 1.8 \times 10^6$	

[a] The energy of each state relative to the ground state is given in parentheses. [b] The k_{ET} values for CS from ^{1}ZnP* and ^{1}C$_{60}$* were determined from the fluorescence lifetimes by using the following equation: $k_{ET} = (1/\tau(\textbf{ZnP-C}_{60})) - (1/\tau(\textbf{ZnP-CONH-ref}$ or $\textbf{C}_{60}\textbf{-ref}))$. The other k_{ET} values for CS and CR were determined by analyzing the rise or decay of C$_{60}^{\bullet-}$ at 1000 nm. [c] The efficiencies (Φ) for each deactivation pathway were estimated on the basis of Schemes 1 and 2. [d] From ref 22. [e] From ref 21. [f] The total quantum yield of CS based on the comparative method. The corresponding value obtained from the kinetic data is given in parentheses.

(absorption ratio of ZnP:C$_{60}$ = 77:23 at 532 nm), are displayed in Figure 2. In detail, the differential spectrum taken immediately after the laser pulse (50 ps delay) is characterized by the bleaching of the porphyrin Q-band absorption at 560 and 600 nm and the stimulating emission from the zinc porphyrin singlet excited state (^{1}ZnP*) at 650 nm. At a delay time of 200 ps, a new transition around 1000 nm grows-in, accompanied by another, but much broader absorption around 650 nm, which importantly differs from the spectral features of the ^{1}ZnP* and triplet excited state (^{3}ZnP*).[21] Based on our previous assignment,[18,21,23,30,31] we ascribe the former and the latter bands to the C$_{60}$ radical anion (C$_{60}^{\bullet-}$)[33] and the zinc porphyrin radical cation (ZnP$^{\bullet+}$),[34] respectively. In accordance with these results we propose the occurrence of a photoinduced ET, evolving from ^{1}ZnP* to the C$_{60}$ and, in turn, creating the **ZnP$^{\bullet+}$-C$_{60}^{\bullet-}$** state. The energy levels in benzonitrile, as extracted from Table 2, are shown in Scheme 1 to illustrate the different relaxation pathways of photoexcited **ZnP-C$_{60}$**. Similar transient absorption spectra, specifically, the spectral fingerprints of ZnP$^{\bullet+}$ and C$_{60}^{\bullet-}$, were obtained in THF and DMF.

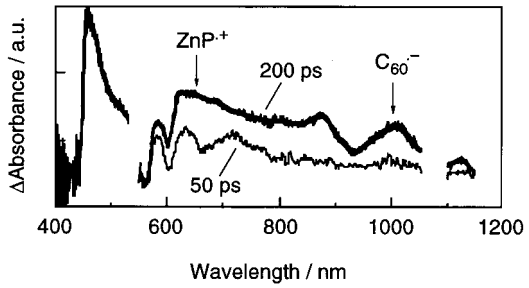

Figure 2. Picosecond time-resolved absorption spectra of **ZnP-C$_{60}$** at a time delay of 50 (thin line) and 200 ps (thick line) excited at 532 nm (absorption ratio of ZnP:C$_{60}$ = 77:23) in argon-saturated benzonitrile. The spectra are normalized at the Soret band for comparison.

Scheme 1. Reaction Scheme and Energy Diagram for **ZnP-C$_{60}$** in Benzonitrile

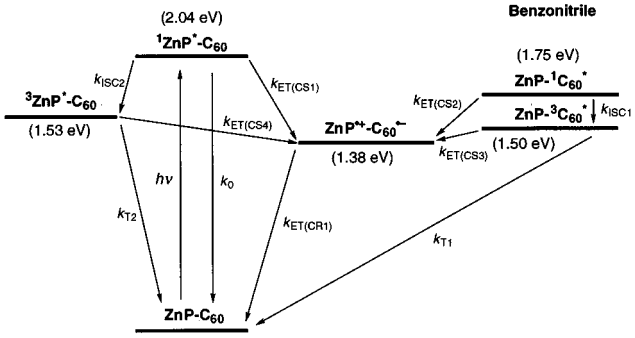

(29) (a) Guldi, D. M.; Maggini, M.; Scorrano, G.; Prato, M. *J. Am. Chem. Soc.* **1997**, *119*, 974. (b) Polese, A.; Mondini, S.; Bianco, A.; Toniolo, C.; Scorrano, G.; Guldi, D. M.; Maggini, M. *J. Am. Chem. Soc.* **1999**, *121*, 3446. (c) Maggini, M.; Guldi, D. M.; Mondini, S.; Scorrano, G.; Paolucci, F.; Ceroni, P.; Roffia, S. *Chem. Eur. J.* **1998**, *4*, 1992. (d) Guldi, D. M.; Luo, C.; Prato, M.; Dietel, E.; Hirsch, A. *Chem. Commun.* **2000**, 373. (e) Guldi, D. M.; Luo, C.; Da Ros, T.; Prato, M.; Dietel, E.; Hirsch, A. *Chem. Commun.* **2000**, 375. (f) Martín, N.; Sánchez, L.; Herranz, M. A.; Guldi, D. M. *J. Phys. Chem. A* **2000**, *104*, 4648. (g) Luo, C.; Guldi, D. M.; Maggini, M.; Menna, E.; Mondini, S.; Kotov, N. A.; Prato, M. *Angew. Chem. Int. Ed.* **2000**, *39*, 3905. (h) Guldi, D. M.; Maggini, M.; Menna, E.; Scorrano, G.; Ceroni, P.; Marcaccio, M.; Paolucci, F.; Roffia, S. *Chem. Eur. J.* **2001**, in press.

(30) (a) Imahori, H.; Hagiwara, K.; Akiyama, T.; Taniguchi, S.; Okada, T.; Sakata, Y. *Chem. Lett.* **1995**, 265. (b) Imahori, H.; Sakata, Y. *Chem. Lett.* **1996**, 199. (c) Imahori, H.; Hagiwara, K.; Aoki, M.; Akiyama, T.; Taniguchi, S.; Okada, T.; Shirakawa, M.; Sakata, Y. *J. Am. Chem. Soc.* **1996**, *118*, 11771. (d) Akiyama, T.; Imahori, H.; Ajavakom, A.; Sakata, Y. *Chem. Lett.* **1996**, 907. (e) Sakata, Y.; Imahori, H.; Tsue, H.; Higashida, S.; Akiyama, T.; Yoshizawa, E.; Aoki, M.; Yamada, K.; Hagiwara, K.; Taniguchi, S.; Okada, T. *Pure Appl. Chem.* **1997**, *69*, 1951. (f) Tamaki, K.; Imahori, H.; Nishimura, Y.; Yamazaki, I.; Shimomura, A.; Okada, T.; Sakata, Y. *Chem. Lett.* **1999**, 227. (g) Imahori, H.; Ozawa, S.; Ushida, K.; Takahashi, M.; Azuma, T.; Ajavakom, A.; Akiyama, T.; Hasegawa, M.; Taniguchi, S.; Okada, T.; Sakata, Y. *Bull. Chem. Soc. Jpn.* **1999**, *72*, 485. (h) Hirayama, D.; Yamashiro, T.; Takimiya, K.; Aso, Y.; Otsubo, T.; Norieda, H.; Imahori, H.; Sakata, Y. *Chem. Lett.* **2000**, 570.

(31) (a) Imahori, H.; Yamada, K.; Hasegawa, M.; Taniguchi, S.; Okada, T.; Sakata, Y. *Angew. Chem. Int. Ed. Engl.* **1997**, *36*, 2626. (b) Higashida, S.; Imahori, H.; Kaneda, T.; Sakata, Y. *Chem. Lett.* **1998**, 605. (c) Tamaki, K.; Imahori, H.; Nishimura, Y.; Yamazaki, I.; Sakata, Y. *Chem. Commun.* **1999**, 625. (d) Imahori, H.; Yamada, H.; Ozawa, S.; Ushida, K.; Sakata, Y. *Chem. Commun.* **1999**, 1165. (e) Imahori, H.; Norieda, H.; Yamada, H.; Nishimura, Y.; Yamazaki, I.; Sakata, Y.; Fukuzumi, S. *J. Am. Chem. Soc.* **2001**, *123*, 100.

(32) (a) Thomas, K. G.; Biju, V.; Guldi, D. M.; Kamat, P. V.; George, M. V. *J. Phys. Chem. B* **1999**, *103*, 8864. (b) Thomas, K. G.; Biju, V.; Guldi, D. M.; Kamat, P. V.; George, M. V. *J. Phys. Chem. A* **1999**, *103*, 10755. (c) Tkachenko, N. V.; Rantala, L.; Tauber, A. Y.; Helaja, J.; Hynninen, P. H.; Lemmetyinen, H. *J. Am. Chem. Soc.* **1999**, *121*, 9378. (d) Tkachenko, N. V.; Vuorimaa, E.; Kesti, T.; Alekseev, A. S.; Tauber, A. Y.; Hynninen, P. H.; Lemmetyinen, H. *J. Phys. Chem. B* **2000**, *104*, 6371. (e) Montforts, F.-P.; Kutzki, O. *Angew. Chem. Int. Ed.* **2000**, *39*, 599. (f) D'Souza, F.; Deviprasad, G. R.; Rahman, M. S.; Choi, J.-p. *Inorg. Chem.* **1999**, *38*, 2157.

(33) (a) Greaney, M. A.; Gorun, S. M. *J. Phys. Chem.* **1991**, *95*, 7142. (b) Dubois, D.; Kadish, K. M.; Flanagan, S.; Haufler, R. E.; Chibante, L. B. F.; Wilson, L. J. *J. Am. Chem. Soc.* **1991**, *113*, 4364. (c) Kato, T.; Kodama, T.; Shida, T.; Nakagawa, T.; Matsui, Y.; Suzuki, S.; Shiromaru, H.; Yamauchi, K.; Achiba, Y. *Chem. Phys. Lett.* **1991**, *180*, 446. (d) Gasyna, Z.; Andrews, L.; Schatz, P. *J. Phys. Chem.* **1992**, *96*, 1525.

(34) (a) Fuhrhop, J.-H.; Mauzerall, D. *J. Am. Chem. Soc.* **1969**, *91*, 4174. (b) Chosrowjan, H.; Taniguchi, S.; Okada, T.; Takagi, S.; Arai, T.; Tokumaru, K. *Chem Phys. Lett.* **1995**, *242*, 644.

Table 3. ET Rate Constants (k_{ET}) for CS, CR, and CSH and the Driving Forces ($-\Delta G^0_{ET}$) in **Fc-ZnP-C$_{60}$**

solvent	initial state[a]	final state[a]	$-\Delta G^0_{ET}$/eV	k_{ET}/s^{-1}[b]	Φ[c]
THF	Fc-^{1}ZnP*−C$_{60}$ (2.07 eV)	Fc-ZnP$^{\bullet+}$-C$_{60}^{\bullet-}$ (1.42 eV)	0.65	$k_{ET(CS1)} = 1.3 \times 10^{10}$[d]	$\Phi_{CS1}(^1ZnP^*) = 0.95$
(ϵ_s=7.58)	Fc-ZnP-^{1}C$_{60}$* (1.75 eV)	Fc-ZnP$^{\bullet+}$-C$_{60}^{\bullet-}$ (1.42 eV)	0.33	$k_{ET(CS2)} = 2.3 \times 10^8$	$\Phi_{CS2}(^1C_{60}^*) = 0.23$
	Fc-^{1}ZnP*-C$_{60}$ (2.07 eV)	Fc$^+$-ZnP$^{\bullet-}$-C$_{60}$ (1.94 eV)	0.13	$k_{ET(CS5)} = 2.4 \times 10^8$[d]	$\Phi_{CS5}(^1ZnP^*) = 0.02$
	Fc-ZnP$^{\bullet+}$-C$_{60}^{\bullet-}$ (1.42 eV)	Fc$^+$-ZnP-C$_{60}^{\bullet-}$ (1.00 eV)	0.42	$k_{ET(CSH1)} = 1.4 \times 10^9$	$\Phi_{CSH1} \sim 1$
	Fc$^+$-ZnP-C$_{60}^{\bullet-}$ (1.00 eV)	Fc-ZnP-C$_{60}$	1.00	$k_{ET(CR2)} = 2.7 \times 10^5$[e]	$\Phi_{CS}(total)$[f] = 0.74
benzonitrile	Fc-^{1}ZnP*-C$_{60}$ (2.04 eV)	Fc-ZnP$^{\bullet+}$-C$_{60}^{\bullet-}$ (1.38 eV)	0.66	$k_{ET(CS1)} = 9.5 \times 10^9$	$\Phi_{CS1}(^1ZnP^*) = 0.90$
(ϵ_s=25.2)	Fc-ZnP-^{1}C$_{60}$* (1.75 eV)	Fc-ZnP$^{\bullet+}$-C$_{60}^{\bullet-}$ (1.38 eV)	0.37	$k_{ET(CS2)} = 5.1 \times 10^8$	$\Phi_{CS2}(^1C_{60}^*) = 0.40$
	Fc-ZnP-^{3}C$_{60}$* (1.50 eV)	Fc-ZnP$^{\bullet+}$-C$_{60}^{\bullet-}$ (1.38 eV)	0.12	$k_{ET(CS3)} = 3.2 \times 10^6$	$\Phi_{CS3}(^3C_{60}^*) = 0.99$
	Fc-^{3}ZnP*-C$_{60}$ (1.53 eV)	Fc-ZnP$^{\bullet+}$-C$_{60}^{\bullet-}$ (1.38 eV)	0.15	$k_{ET(CS4)} > 3.2 \times 10^6$	$\Phi_{CS4}(^3ZnP^*) = 0.99$
	Fc-^{1}ZnP*−C$_{60}$ (2.04 eV)	Fc$^+$−ZnP$^{\bullet-}$-C$_{60}$ (1.81 eV)	0.23	$k_{ET(CS5)} = 5.5 \times 10^8$	$\Phi_{CS5}(^1ZnP^*) = 0.05$
	Fc-ZnP$^{\bullet+}$-C$_{60}^{\bullet-}$ (1.38 eV)	Fc$^+$-ZnP-C$_{60}^{\bullet-}$ (1.03 eV)	0.35	$k_{ET(CSH1)} = 2.8 \times 10^9$	$\Phi_{CSH1} \sim 1$
	Fc-ZnP$^{\bullet+}$-C$_{60}^{\bullet-}$ (1.38 eV)	Fc-ZnP-C$_{60}$	1.38	$k_{ET(CR1)} = 1.3 \times 10^6$	
	Fc$^+$-ZnP-C$_{60}^{\bullet-}$ (1.03 eV)	Fc-ZnP-C$_{60}$	1.03	$k_{ET(CR2)} = 1.3 \times 10^5$[e]	$\Phi_{CS}(total)^f = 0.82$ (0.99)
DMF	Fc$^+$-ZnP-C$_{60}^{\bullet-}$ (0.91 eV)	Fc-ZnP-C$_{60}$	0.91	$k_{ET(CR2)} = 6.3 \times 10^4$[e]	$\Phi_{CS}(total)^f = 0.36$
(ϵ_s=36.7)					

[a] The energy of each state relative to the ground state is given in parentheses. [b] The k_{ET} values for CS from ^{1}ZnP* and ^{1}C$_{60}$* were determined from the fluorescence lifetimes by using the following equation: $k_{ET} = (1/\tau$ (**Fc-ZnP-C$_{60}$** or **ZnP-Fc**)) − ($1/\tau$(**ZnP-Fc** or **ZnP-CONH-ref** or **C$_{60}$-ref**)). The other k_{ET} values for CS, CR, and CSH were determined by analyzing the rise and decay of C$_{60}^{\bullet-}$ at 1000 nm and the decay of ZnP$^{\bullet+}$ at 660 nm, respectively. [c] The efficiencies (Φ) for each deactivation pathway were estimated on the basis of Scheme 3. [d] From ref 19. [e] From ref 18. [f] The total quantum yield of CS based on the comparative method. The corresponding value obtained from the kinetic data is given in parentheses.

Table 4. ET Rate Constants (k_{ET}) for CR and the Driving Forces ($-\Delta G^0_{ET}$) in **Fc-H$_2$P-C$_{60}$** and **ZnP-H$_2$P-C$_{60}$**

solvent	initial state[a]	final state[a]	$-\Delta G^0_{ET}$/eV	k_{ET}/s^{-1}[b]	Φ_{CS}(total)[c]
THF	ZnP$^{\bullet+}$-H$_2$P-C$_{60}^{\bullet-}$ (1.37 eV)	ZnP-H$_2$P-C$_{60}$	1.37	$k_{ET(CR2)} = 2.9 \times 10^4$	$\Phi_{CS}(total) = 0.26$
(ϵ_s = 7.58)					
benzonitrile	Fc$^+$-H$_2$P-C$_{60}^{\bullet-}$ (1.03 eV)	Fc-H$_2$P-C$_{60}$	1.03	$k_{ET(CR2)} = 1.2 \times 10^5$	$\Phi_{CS}(total) = 0.25$
(ϵ_s = 25.2)	ZnP$^{\bullet+}$-H$_2$P-C$_{60}^{\bullet-}$ (1.34 eV)	ZnP-H$_2$P-C$_{60}$	1.34	$k_{ET(CR2)} = 4.8 \times 10^4$[d]	$\Phi_{CS}(total) = 0.40$
DMF	Fc$^+$-H$_2$P-C$_{60}^{\bullet-}$ (0.91 eV)	Fc-H$_2$P-C$_{60}$	0.91	$k_{ET(CR2)} = 5.3 \times 10^4$	$\Phi_{CS}(total) = 0.27$
(ϵ_s = 36.7)	ZnP$^{\bullet+}$-H$_2$P-C$_{60}^{\bullet-}$ (1.17 eV)	ZnP-H$_2$P-C$_{60}$	1.17	$k_{ET(CR2)} = 5.0 \times 10^4$	$\Phi_{CS}(total) = 0.21$

[a] The energy of each state relative to the ground state is given in parentheses. [b] The k_{ET} values for CR were determined by analyzing the decay of C$_{60}^{\bullet-}$ at 1000 nm. [c] The total quantum yield of CS based on the comparative method. [d] From ref 21.

Table 5. Fluorescence Lifetimes (τ) of **ZnP-C$_{60}$**, **Fc-ZnP-C$_{60}$**, and the Reference Compounds in THF, Benzonitrile, and DMF[a]

	lifetimes (τ)/ns				
	λ_{obs} [THF (ϵ_s = 7.58)]		λ_{obs} [benzonitrile (ϵ_s = 25.2)]		λ_{obs} [DMF (ϵ_s = 36.7)]
compd	610 nm	720 nm	610 nm	720 nm	610 nm
ZnP-C$_{60}$	0.075[b]	0.78	0.10	0.76	0.075[b]
ZnP-CONH-ref	2.1[b]		2.0		2.0[b]
C$_{60}$-ref		1.3		1.3	
Fc-ZnP-C$_{60}$	0.074[c]	1.0	0.095	0.78	
ZnP-Fc	1.4[c]		0.95		

[a] λ_{ex} = 410 nm. [b] From ref 22. [c] From ref 19.

Next we measured the fluorescence lifetimes (τ) of **ZnP-C$_{60}$**, **ZnP-CONH-ref**, and **C$_{60}$-ref** with a time-correlated single-photon-counting apparatus by using a 410 nm excitation (absorption ratio (**ZnP-C$_{60}$**) of ZnP:C$_{60}$ = 90:10 in benzonitrile). These experiments allowed probing the decay dynamics of the photoexcited fullerene and porphyrin cores separately. Therefore, the fluorescence decay was monitored at 610 and 720 nm, relating to the emission of the porphyrin (λ_{max} = 605, 655 nm)[30c] and the C$_{60}$ (λ_{max} = 720 nm)[30c] moiety, respectively. In general, the fluorescence decay curves were well fitted by a single-exponential decay component (see Table 5).

On the basis of the fluorescence lifetimes (λ_{obs} = 610 nm) in benzonitrile, the ET rate constants ($k_{ET(CS1)} = 9.5 \times 10^9$ s^{-1}; see Supporting Information (p S8)) for CS from ^{1}ZnP* and the efficiency ($\Phi_{CS1}(^1ZnP^*) = 0.95$) of **ZnP$^{\bullet+}$-C$_{60}^{\bullet-}$** formation were determined. Nearly the same $k_{ET(CS1)}$ values were found in THF (1.3×10^{10} s^{-1})[22] and DMF (1.3×10^{10} s^{-1})[22] (Table 2). Since there is considerable excitation of the fullerene core that cannot be avoided, we would like to emphasize that CS, and, thereby, generation of **ZnP$^{\bullet+}$-C$_{60}^{\bullet-}$**, also occurs between the ZnP ground state and the C$_{60}$ singlet excited state (^{1}C$_{60}$*). The ET rate constant ($k_{ET(CS2)}$; see Supporting Information (p S8)) and the efficiency of **ZnP$^{\bullet+}$-C$_{60}^{\bullet-}$** formation ($\Phi_{CS2}(^1C_{60}^*)$) from the ^{1}C$_{60}$* were determined as 5.5×10^8 s^{-1} and 0.42 in benzonitrile, respectively (Table 2).

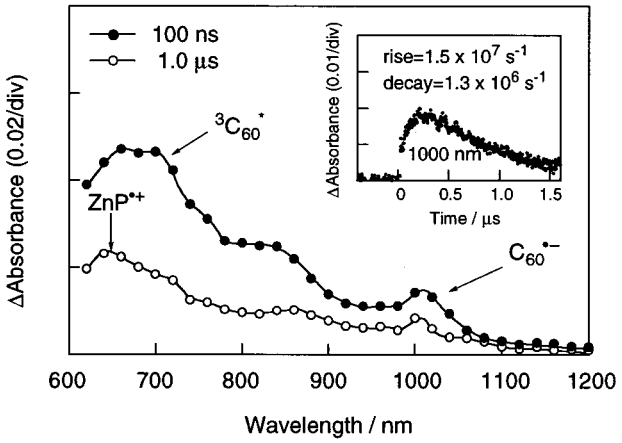

Figure 3. Nanosecond time-resolved absorption spectra of **ZnP-C$_{60}$** in argon-saturated benzonitrile excited at 532 nm (absorption ratio of ZnP:C$_{60}$ = 77:23). The delay times between the excitation and measurement are indicated on the left. The time profile of absorbance at 1000 nm is shown as the inset.

Formation of C$_{60}^{\bullet-}$ (1000 nm) and ZnP$^{\bullet+}$ (broad absorption around 650 nm) was further substantiated (Figure 3) by a set of complementary nanosecond experiments. Interestingly, in addition to the C$_{60}^{\bullet-}$ and ZnP$^{\bullet+}$ characteristics, we also noted evidence for the fullerene triplet state (^{3}C$_{60}$*), as inferred by the 700 nm absorption maximum.[21] In line with this fullerene triplet formation, the time profile at 1000 nm due to C$_{60}^{\bullet-}$ reveals

a rise and a decay component with rate constants of 1.5×10^7 and 1.3×10^6 s^{-1}, respectively (Figure 3, inset). Considering the energy diagram in a polar solvent (shown for benzonitrile in Scheme 1), photoinduced CS evolving from the fullerene triplet state is thermodynamically exothermic and thus likely to occur. In accordance with this conclusion, based on energetics, is the fact that the rise in absorbance at 1000 nm ($(k_{ET(CS3)})$ of 1.5×10^7 s^{-1}) matches exactly the C_{60} triplet decay at 700 nm. Given the intrinsic rate constant for the decay of $^3C_{60}$* ($k_{T1} = 4.0 \times 10^4$ s^{-1}),[21] the efficiency of formation of the charge-separated state from $^3C_{60}$* ($\Phi_{CS3}(^3C_{60}$*); see Supporting Information (p S8)) is nearly unity (Table 2).

Since the energy level of the porphyrin triplet excited state (^{3}ZnP*: 1.53 eV)[21] is slightly higher than that of the corresponding fullerene triplet state ($^3C_{60}$*: 1.50 eV),[21] the charge-separated state may also be generated via the transient ^{3}ZnP* through ET with a rate constant ($k_{ET(CS4)}$) of $>1.5 \times 10^7$ s^{-1}. Taking the decay rate constant ($k_{T2} = 2.3 \times 10^4$ s^{-1})[21] of a zinc-*meso*-tetraphenylporphyrin (ZnTPP) triplet excited state into account, the efficiency of formation of the charge-separated state from ^{3}ZnP* ($\Phi_{CS4}(^3$ZnP*); see Supporting Information (p S8)) should also be close to unity (Table 2).

On the basis of the quantum yields of porphyrin (Φ_{ISC2}-(^{1}ZnP*) = 0.88)[21] and C_{60} ($\Phi_{ISC1}(^1C_{60}$*) = 0.98)[21] triplet excited state formation, the total efficiency of **ZnP**$^{\bullet+}$-**C**$_{60}^{\bullet-}$ formation ($\Phi_{CS(total)}$(**ZnP-C$_{60}$**)) from the initial excited states in benzonitrile is estimated to be 0.99 (Table 2).[35] This appraisal is consistent with the high quantum yield for CS of 0.85 determined from the nanosecond time-resolved transient spectra (monofunctionalized $C_{60}^{\bullet-}$ ($\epsilon_{1000nm} = 4700$ M^{-1} cm^{-1},[36] see Supporting Information).[37]

The resulting charge-separated state recombines to regenerate the singlet ground state. From the decay kinetics at 1000 nm a rate constant ($k_{ET(CR1)}$) of 1.3×10^6 s^{-1} is deduced for a benzonitrile solution.[21] Remarkably, this rate is nearly 4 orders of magnitude slower than the fastest occurring CS, namely, that stemming from ^{1}ZnP* ($k_{ET(CS1)} = 9.5 \times 10^9$ s^{-1}). Such a fast CS, combined with a slow CR, in the **ZnP-C$_{60}$** dyad in polar solvents is in clear contrast to conventional porphyrin−quinone and −diimide linked dyads, where the CR rates are even faster than the CS rates in polar solvents.[2,13,16]

The photodynamical behavior of the **ZnP-C$_{60}$** dyad in THF and DMF is similar to that described in benzonitrile (Table 2). A possible explanation for this analogy is based on the corresponding energy levels. In particular, the energies of the excited states (i.e., ^{1}ZnP* (2.04−2.07 eV), ^{3}ZnP* (1.53 eV), $^1C_{60}$* (1.75 eV), and $^3C_{60}$* (1.50 eV)) are substantially higher than the energy of the charge-separated state in THF (1.42 eV), benzonitrile (1.38 eV), and DMF (1.21 eV). This, in turn, guarantees high driving forces for the associated CS and CR processes.

(b) H$_2$P-C$_{60}$: A similar picture can be summarized for the **H$_2$P-C$_{60}$** dyad in benzonitrile (Scheme 2). CS from the freebase porphyrin singlet excited state (^1H_2P* (1.89 eV)) to C_{60} in benzonitrile occurs to yield **H$_2$P**$^{\bullet+}$-**C**$_{60}^{\bullet-}$ (1.59 eV) with a rate constant ($k_{ET(CS1)}$) of 5.2×10^9 s^{-1} (Table 2).[21] In contrast to the **ZnP-C$_{60}$** dyad, the resulting charge-separated state decays with a rate constant of 2.2×10^7 s^{-1}, generating, however, eventually the porphyrin triplet state (^3H_2P*) rather than the ground state.[21] The CS rate starting from the $^1C_{60}$* ($k_{ET(CS2)}$) could not be determined by the fluorescence lifetime measurements because of the interference caused by the strong H_2P emission ($\lambda_{max(em)} = 655$, 720 nm), which overlaps extensively with the much weaker fullerene emission ($\lambda_{max(em)} = 720$ nm). The unquenched **H$_2$P-^{1}C$_{60}$*** (1.75 eV) undergoes an intersystem crossing to **H$_2$P-^{3}C$_{60}$*** (1.50 eV), which then decays either to the ground state or to the **^{3}H$_2$P*-C$_{60}$** state (1.40 eV).[21]

Scheme 2. Reaction Scheme and Energy Diagram for **H$_2$P-C$_{60}$** in Benzonitrile

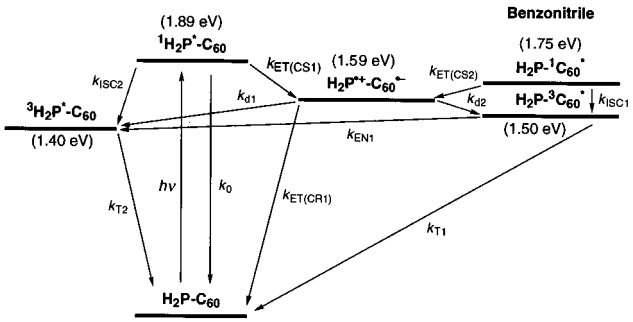

Scheme 3. Reaction Scheme and Energy Diagram for **Fc-ZnP-C$_{60}$** in Benzonitrile

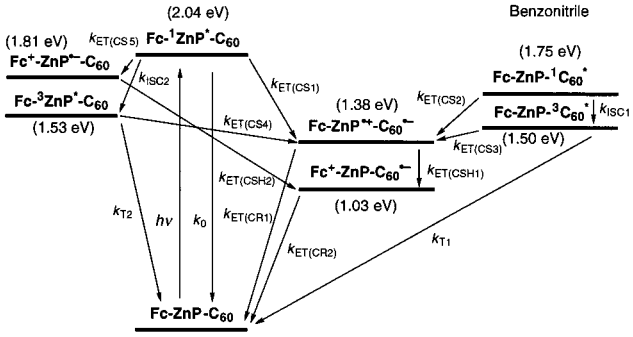

Photophysics of Porphyrin−Fullerene Linked Triads. (a) Fc-ZnP-C$_{60}$: The energy levels in benzonitrile, which are expected to be of significance for the photoinduced ET reactions in **Fc-ZnP-C$_{60}$**, are taken from the data summarized in Table 3 and are diagrammed in Scheme 3.

Figure 4a depicts, as a representative example, the picosecond absorption spectra of **Fc-ZnP-C$_{60}$** in a benzonitrile solution (absorption ratio of Fc:ZnP:C_{60} = 1:75:24 at 532 nm). Generally, the spectral behavior of **Fc-ZnP-C$_{60}$** is similar to that discussed above for **ZnP-C$_{60}$** (Figure 2). From this analogy we may already gather that again two major CS pathways prevail, which produce in both cases **Fc-ZnP**$^{\bullet+}$-**C**$_{60}^{\bullet-}$ (Scheme 3). First, a fast step occurs, which involves CS from ^{1}ZnP* to C_{60} ($k_{ET(CS1)} = 9.5 \times 10^9$ s^{-1}, $\Phi_{CS1}(^1$ZnP*) = 0.90), and second, a slower reaction between ZnP and $^1C_{60}$* ($k_{ET(CS2)} = 5.1 \times 10^8$ s^{-1}, Φ_{CS2}-($^1C_{60}$*) = 0.40). The rate constants ($k_{ET(CS1)}$ and $k_{ET(CS2)}$) and the efficiencies of **Fc-ZnP**$^{\bullet+}$-**C**$_{60}^{\bullet-}$ formation from the ^{1}ZnP* ($\Phi_{CS1}(^1$ZnP*)) and from the $^1C_{60}$* ($\Phi_{CS2}(^1C_{60}$*)) were determined as described for **ZnP-C$_{60}$** (see Supporting Information (p S9)). The fluorescence lifetime measurements of the **ZnP-Fc** reference and **ZnP-CONH-ref** in benzonitrile (Table 5) indicate, however, that yet another CS may occur, namely, from the ferrocene to the ^{1}ZnP* to produce **Fc**$^+$-**ZnP**$^{\bullet-}$ ($k_{ET(CS5)} = 5.5 \times 10^8$ s^{-1}; See Supporting Information (p S9)). The CS5 is slower by a factor of ∼1/20 than the analogous process involving C_{60} in **Fc-ZnP-C$_{60}$** ($k_{ET(CS1)} = 9.5 \times 10^9$ s^{-1}). Thus,

(35) Φ_{CS}(total)(**ZnP-C$_{60}$**) = (absorption ratio of ZnP) × [$\Phi_{CS1}(^1$ZnP*) + $\Phi_{ISC2}(^1$ZnP*) × $\Phi_{CS4}(^3$ZnP*)] + (absorption ratio of C_{60}) × [$\Phi_{CS2}(^1C_{60}$*) + $\Phi_{ISC1}(^1C_{60}$*) × $\Phi_{CS3}(^3C_{60}$*)] = 0.77 × [0.95 + 0.05 × 0.88 × 1] + 0.23 × [0.40 + 0.60 × 0.98 × 1] = 0.99.

(36) Luo, C.; Fujitsuka, M.; Huang, C.-H.; Ito, O. *Phys. Chem. Chem. Phys.* **1999**, *1*, 2923.

(37) The difference in the Φ_{CS}(total) values, obtained from the comparative method and the kinetic analysis, may largely stem from the experimental uncertainty in the extinction coefficients of the transient species.

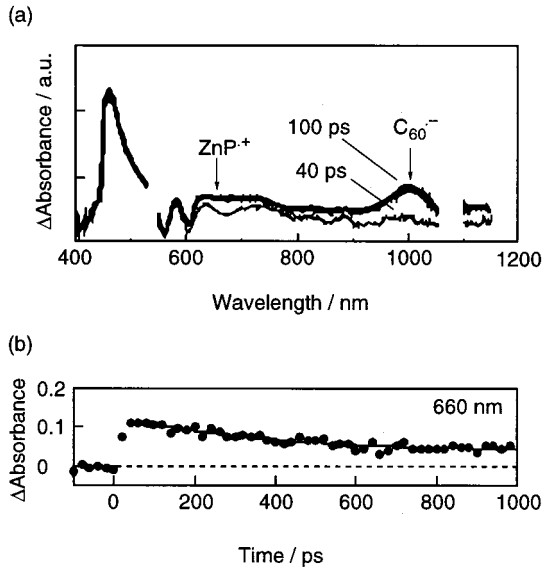

Figure 4. (a) Picosecond time-resolved absorption spectra of **Fc-ZnP-C$_{60}$** at delay time of 40 (thin line) and 100 ps (thick line) excited at 532 nm (absorption ratio of Fc:ZnP:C_{60} = 1:75:24) in argon-saturated benzonitrile. The spectra are normalized at the Soret band for comparison. (b) Time profile of absorbance at 660 nm. The solid line is a simulated curve using $(\tau(ZnP^{\bullet+}))^{-1} = 2.8 \times 10^9\ s^{-1}$.

this deactivation pathway to generate **Fc$^+$-ZnP$^{\bullet-}$-C$_{60}$** (Φ_{CS5}-(^{1}ZnP*) = 0.05; see Supporting Information (p S9)) is rather negligible, although the charge-separated state could then undergo an exothermic charge shift (CSH) ($-\Delta G^0_{ET(CSH2)}$ = 0.78 eV) to generate **Fc$^+$-ZnP-C$_{60}^{\bullet-}$** efficiently.

While nanosecond transient absorption studies following laser excitation of **Fc-ZnP-C$_{60}$** reveal unambiguously the $C_{60}^{\bullet-}$ fingerprint (ca. 1000 nm), as in the case of **ZnP-C$_{60}$** (Figure 3), none of the $ZnP^{\bullet+}$ attributes (650 nm) could be detected on this time scale (see Supporting Information (p S11)). Taking the small molar absorption coefficient of the ferricenium ion ($\lambda_{max} \sim 800$ nm ($\epsilon \sim 1000\ M^{-1}\ cm^{-1}$)) into account,[38] it is concluded that the transient **Fc-ZnP$^{\bullet+}$-C$_{60}^{\bullet-}$** state undergoes a subsequent and rapid CSH to generate the final **Fc$^+$-ZnP-C$_{60}^{\bullet-}$** state. The CSH rate constant ($k_{ET(CSH1)}$) in benzonitrile (see Supporting Information (p S9)) was determined as $2.8 \times 10^9\ s^{-1}$ by using the $k_{ET(CR1)}$(**ZnP-C$_{60}$**) ($1.3 \times 10^6\ s^{-1}$) value in Table 2 and monitoring the decay of the $ZnP^{\bullet+}$ ($(\tau(ZnP^{\bullet+}))^{-1} = 2.8 \times 10^9\ s^{-1}$) around 650 nm (Figure 4b). The efficiency of CSH from the Fc to the $ZnP^{\bullet+}$ in **Fc-ZnP$^{\bullet+}$-C$_{60}^{\bullet-}$** (Φ_{CSH1}) (see Supporting Information (p S9)) was found to be nearly unity (Table 3).

The time profile of **Fc-ZnP-C$_{60}$** at 1000 nm displays a rise and a decay component with underlying rate constants of 3.2×10^6 and $1.3 \times 10^5\ s^{-1}$, respectively (see Supporting Information (p S11)). A closer inspection of the energy level diagram in a polar solvent (Scheme 3; benzonitrile) reveals that it is energetically feasible to generate **Fc-ZnP$^{\bullet+}$-C$_{60}^{\bullet-}$** from $^3C_{60}$*. This process is ascribed to the rise in absorbance at 1000 nm from which we derived a rate constant ($k_{ET(CS3)}$) of $3.2 \times 10^6\ s^{-1}$. Taking the above facts into account, the efficiency regarding the formation of the charge-separated state from $^3C_{60}$* ($\Phi_{CS3}(^3C_{60}*)$) (see Supporting Information (p S9)) can be approximated to be 0.99 (Table 3).

Since the energy level of the porphyrin triplet excited state (^{3}ZnP*: 1.53 eV)[21] is slightly higher than that of the corresponding fullerene triplet state ($^3C_{60}$*: 1.50 eV),[21] the charge-separated state may also be generated via the transient ^{3}ZnP* through ET with a rate constant ($k_{ET(CS4)}$) of $>3.2 \times 10^6\ s^{-1}$, as in the case of **ZnP-C$_{60}$**. Taking the decay rate constant ($k_{T2} = 2.3 \times 10^4\ s^{-1}$)[21] of a zinc-*meso*-tetraphenylporphyrin (ZnTPP) triplet excited state into account, the efficiency of formation of the charge-separated state from ^{3}ZnP* ($\Phi_{CS4}(^3ZnP*)$) should also be 0.99 (see Supporting Information (p S9)).

Assuming that the efficiency of **Fc$^+$-ZnP-C$_{60}^{\bullet-}$** formation ($\Phi_{CS5} \times \Phi_{CSH2}$) from ^{1}ZnP* via **Fc$^+$-ZnP$^{\bullet-}$-C$_{60}$**, which is a minor CS pathway, is unity and that the overall absorption of the ferrocene moiety is negligible, the total efficiency of **Fc$^+$-ZnP-C$_{60}^{\bullet-}$** formation (Φ_{CS}(total)) from the initial excited states, as determined from the k_{ET} and Φ_{CS} values in Table 3, is 0.99 (Table 3).[39] This is consistent with the quantum yield obtained from the transient absorption spectra (Φ_{CS}(total) = 0.82).[36,37] Thus, even in benzonitrile the **Fc-ZnP-C$_{60}$** triad produces, upon photoexcitation, a long-lived charge-separated state (7.5 μs) with an extremely high efficiency (0.99). This can be understood reasonably by the fact that C_{60} has a small reorganization energy in ET, which, in turn, assists in accelerating CS and CSH reaction, while decelerating CR processes.

A similar photodynamical behavior was noted in THF and DMF solutions (Table 3). For instance, the CSH rate constant ($k_{ET(CSH1)}$) and the efficiency of the CSH (Φ_{CSH1}) in THF were found to be $1.4 \times 10^9\ s^{-1}$ and nearly unity, respectively.

By analyzing the decay kinetics of the $C_{60}^{\bullet-}$ fingerprint at 1000 nm, the ET rate constants for CR in **Fc$^+$-ZnP-C$_{60}^{\bullet-}$** ($k_{ET(CR2)}$) were determined as 2.7×10^5 (THF), 1.3×10^5 (benzonitrile), and $6.3 \times 10^4\ s^{-1}$ (DMF).[18] The total quantum yields of CS (Φ_{CS}(total)) in **Fc-ZnP-C$_{60}$** were found to be 0.74 in THF and 0.36 in DMF by the comparative method from the corresponding transient absorption spectra (Table 3).[36]

(b) Fc-H$_2$P-C$_{60}$: As a consequence of the poor signal-to-noise ratio, picosecond time-resolved transient absorption studies with **Fc-H$_2$P-C$_{60}$** in benzonitrile were unsuccessful with respect to any assignment of a $C_{60}^{\bullet-}$ fingerprint (ca. 1000 nm). Instead, nanosecond time-resolved transient absorption spectra of **Fc-H$_2$P-C$_{60}$** (absorption ratio of Fc:H_2P:C_{60} = 1:86:13 at 532 nm) in benzonitrile were recorded (see Supporting Information (p S12)). The spectral features of **Fc-H$_2$P-C$_{60}$** are quite different from those of **Fc-ZnP-C$_{60}$**. In particular, a characteristic absorption appears around 700 and 800 nm, due to $^3C_{60}$* and ^3H_2P*,[21] respectively, in addition to the weak absorption around 1000 nm originating from $C_{60}^{\bullet-}$. Absorption due to the freebase porphyrin radical cation ($H_2P^{\bullet+}$ ($\sim$700 nm))[40] could not be detected within the time domain of >10 ns.

In reference to the energy level diagram shown in Scheme 4, the deactivation pathways of photoexcited **Fc-H$_2$P-C$_{60}$** in benzonitrile can be proposed as follows. First, an initial ET to C_{60} (CS1) follows the instantaneous population of **Fc-^{1}H$_2$P*-C$_{60}$** (1.89 eV), to yield, in turn, **Fc-H$_2$P$^{\bullet+}$-C$_{60}^{\bullet-}$** (1.59 eV).[41] The resulting charge-separated state reacts essentially via three different decay pathways with respective rate constants, namely, (i) (k_{d1}) to **Fc-^{3}H$_2$P*-C$_{60}$** (1.40 eV), (ii) (k_{d2}) to **Fc-H$_2$P-^{3}C$_{60}$*** (1.50 eV), and (iii) ($k_{ET(CSH1)}$) to **Fc$^+$-H$_2$P-C$_{60}^{\bullet-}$** (1.03 eV).

(38) Fukuzumi, S.; Mochizuki, S.; Tanaka, T. *Inorg. Chem.* **1989**, *28*, 2459.

(39) Φ_{CS}(total)(**Fc-ZnP-C$_{60}$**) = (absorption ratio of ZnP) × {[Φ_{CS1}-(^{1}ZnP*) + $\Phi_{ISC2}(^1ZnP*) \times \Phi_{CS4}(^3ZnP*)$] × [$k_{ET(CSH1)}/(k_{ET(CR1)} + k_{ET(CSH1)})$] + $\Phi_{ET(CS5)}(^1ZnP*) \times \Phi_{ET(CSH2)}(^1ZnP*)$} + (absorption ratio of C_{60}) × [$\Phi_{CS2}(^1C_{60}*) + \Phi_{ISC1}(^1C_{60}*) \times \Phi_{CS3}(^3C_{60}*)$] × [$k_{ET(CSH1)}/(k_{ET(CR1)} + k_{ET(CSH1)})$] = 0.76 × {[0.90 + 0.05 × 0.88 × 0.99] × 1 + 0.05 × 1} + 0.24 × [0.40 + 0.60 × 0.98 × 0.99] × 1 = 0.99.

(40) Gasyna, Z.; Browett, W. R.; Stillman, M. J. *Inorg. Chem.* **1985**, *24*, 2440.

Scheme 4. Reaction Scheme and Energy Diagram for **Fc-H$_2$P-C$_{60}$** in Benzonitrile

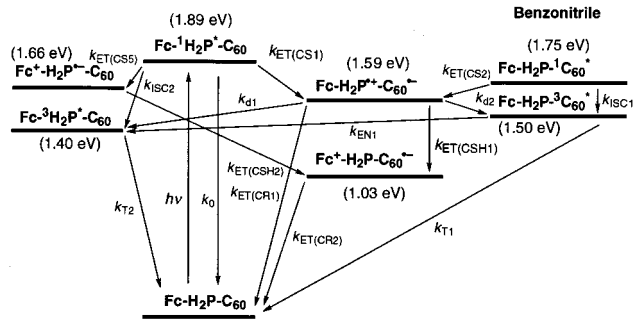

Scheme 5. Reaction Scheme and Energy Diagram for **ZnP-H$_2$P-C$_{60}$** in Benzonitrile

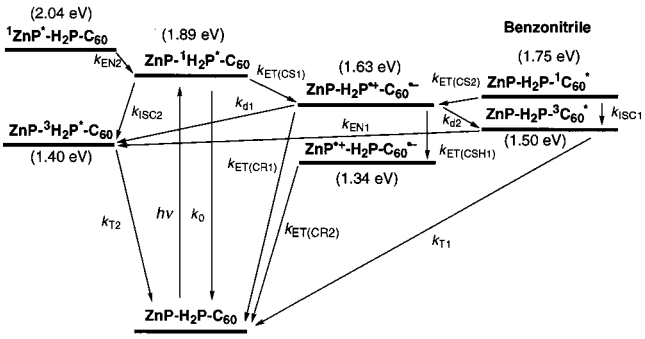

CS from the **Fc-H$_2$P-^{1}C$_{60}$*** (CS2) could not be confirmed by fluorescence lifetime measurements, because of the extensive overlap between the freebase porphyrin emission ($\lambda_{max(em)}$ = 655, 720 nm) and the C_{60} emission ($\lambda_{max(em)}$ = 720 nm). This is, in essence, similar to the **H$_2$P-C$_{60}$** case mentioned above. However, the energy levels in Scheme 4 show that a photoinduced CS reaction even between the fullerene singlet excited state and the porphyrin (CS2) is a possibility that would produce **Fc-H$_2$P$^{\bullet+}$-C$_{60}^{\bullet-}$**. In contrast, the unquenched **Fc-H$_2$P-^{1}C$_{60}$*** (1.75 eV) undergoes an intersystem crossing (ISC1) to the **Fc-H$_2$P-^{3}C$_{60}$*** (1.50 eV), which decays either to the ground state or the **Fc-^{3}H$_2$P*-C$_{60}$** state (1.40 eV). The ET rate constant for CR2 ($k_{ET(CR2)}$) and the total quantum yields for CS (Φ_{CS}(total)) in **Fc-H$_2$P-C$_{60}$** were determined from the transient spectra[36] as 1.2×10^5 s^{-1} and 0.25 in benzonitrile and 5.3×10^4 s^{-1} and 0.27 in DMF, respectively (Table 4).

(c) ZnP-H$_2$P-C$_{60}$: We reported the photophysics of **ZnP-H$_2$P-C$_{60}$** in benzonitrile elsewhere in depth (Scheme 5).[21] Briefly, an initial singlet−singlet energy transfer (EN) from ^{1}ZnP* (2.04 eV) to H$_2$P (1.89 eV) ($k_{EN2} = 1.5 \times 10^{10}$ s^{-1}) is followed by a sequential ET relay evolving from the **ZnP-^{1}H$_2$P*-C$_{60}$** (CS1) to yield **ZnP-H$_2$P$^{\bullet+}$-C$_{60}^{\bullet-}$** (1.63 eV) and subsequently **ZnP$^{\bullet+}$-H$_2$P-C$_{60}^{\bullet-}$** (1.34 eV) via CSH1 in competition with the back ET to the ground state ($k_{ET(CR1)}$) and the porphyrin and C_{60} triplet excited states (k_{d1} and k_{d2}). Thereby, the individual rate constants $k_{ET(CS1)}$ and $k_{ET(CSH1)}$ were 7.0×10^9 and 2.2×10^9 s^{-1}, respectively.[21] The final charge-separated state, formed in moderate quantum yields (0.40), decays directly to the ground state with a rate constant ($k_{ET(CR2)}$) of 4.8×10^4 s^{-1} as analyzed from the decay kinetics of the $C_{60}^{\bullet-}$ absorption (ca. 1000 nm) (Table 4).[21] While in benzonitrile the ET rate ($k_{ET(CR2)}$) for CR is somewhat slower than that in DMF (5.0×10^4 s^{-1}); it was found to be, however, faster in THF (2.9×10^4 s^{-1}). The total quantum yields of CS in **ZnP-H$_2$P-C$_{60}$** (Φ_{CS}(total)) were estimated from the transient absorption spectra[36] as 0.26 in THF and 0.21 in DMF, respectively (Table 4). In addition, CS2 was also found to occur from H$_2$P to ^{1}C$_{60}$* (1.75 eV) to generate **ZnP-H$_2$P$^{\bullet+}$-C$_{60}^{\bullet-}$** (1.63 eV), followed by a subsequent CSH1 to lead to **ZnP$^{\bullet+}$-H$_2$P-C$_{60}^{\bullet-}$**.[21]

Driving Force Dependence of Photoinduced CS and CR Rates. The lifetimes (τ_{CR}) of the charge-separated states (i.e., **ZnP$^{\bullet+}$-C$_{60}^{\bullet-}$**, **Fc$^+$-ZnP-C$_{60}^{\bullet-}$**, **Fc$^+$-H$_2$P-C$_{60}^{\bullet-}$**, and **ZnP$^{\bullet+}$-H$_2$P-C$_{60}^{\bullet-}$**)[42] can be correlated with the solvent polarity. In the case of **ZnP-C$_{60}$** (τ = 2.7 (THF), 0.78 (benzonitrile), 0.57 μs (DMF)) and **ZnP-H$_2$P-C$_{60}$** (τ = 34 (THF), 21 (benzonitrile), 20 μs (DMF)) the lifetimes clearly decrease as the solvent polarity increases (Table 6). However, since the driving force of CR decreases (Tables 2 and 4) with an increase in the solvent polarity, the observed trends in the lifetimes show that the associated ET rate constants are in the inverted region of the Marcus parabola:[1−7,11b,13,16] in other words, as the driving force decreases the rate constants of CR increase (the lifetimes of the charge-separated states decrease). In contrast, the lifetimes of the **Fc$^+$-ZnP-C$_{60}^{\bullet-}$** ion pairs (τ = 3.7 (THF), 7.5 (benzonitrile), 16 μs (DMF)) and the **Fc$^+$-H$_2$P-C$_{60}^{\bullet-}$** ion pairs (τ = 8.3 (benzonitrile), 19 μs (DMF)) grows gradually from the moderately to the strongly polar solvents,[43] indicating that these CR rates are in the normal region of the Marcus curve (Table 6).[44] In this case, as the driving force for CR increases, the rate constants for CR also increase. In general, the driving forces of the CR processes in **ZnP$^{\bullet+}$-H$_2$P-C$_{60}^{\bullet-}$** (1.17−1.37 eV) and **ZnP$^{\bullet+}$-C$_{60}^{\bullet-}$** (1.21−1.42 eV) are markedly larger than those in the corresponding **Fc$^+$-ZnP-C$_{60}^{\bullet-}$** and **Fc$^+$-H$_2$P-C$_{60}^{\bullet-}$** pairs in the normal region (0.91−1.03 eV). Thus, these thermodynamic differences support the above assignment regarding the CR kinetics being either in the normal or inverted region of the Marcus parabola.

To quantify the driving force dependence on the ET rate constants (k_{ET}), eq 3 was employed, where V is the electronic coupling matrix element, k_B is the Boltzmann constant, h is the Planck constant, and T is the absolute temperature.[45] Figure 5 shows the logk_{ET} versus $-\Delta G^0_{ET}$ plots for the different donor−acceptor arrays.

$$k_{ET} = \left(\frac{4\pi^3}{h^2 \lambda k_B T}\right)^{1/2} V^2 \exp\left[-\frac{(\Delta G^0_{ET} + \lambda)^2}{4\lambda k_B T}\right] \qquad (3)$$

The best fits of eq 3 provide λ = 0.66 eV and V = 3.9 cm^{-1} for **ZnP-C$_{60}$**.[46,47] It should be noted that in **ZnP-C$_{60}$** the CS

(41) The fluorescence lifetime of **H$_2$P-Fc** in THF indicates photoinduced ET from the ferrocene to the ^{1}H$_2$P* to produce **H$_2$P$^{\bullet-}$-Fc$^+$** (1.66 eV).[19] However, the ET from the ferrocene to the ^{1}H$_2$P* (7.4×10^7 s^{-1}) is slower by a factor of ~1/8 than that from the ^{1}H$_2$P* to the C_{60} (6.1×10^8 s^{-1}).[19] Thus, the deactivation pathway to generate **Fc$^+$-H$_2$P$^{\bullet-}$-C$_{60}$** is also minor, although the charge-separated state would undergo CSH to the C_{60} to generate **Fc$^+$-H$_2$P-C$_{60}^{\bullet-}$** eventually.

(42) The time-absorption profiles were fitted as a single-exponential decay, which, in turn, allows excluding any intermolecular ET processes under the present conditions.

(43) Osuka, A.; Nakajima, S.; Maruyama, K.; Mataga, N.; Asahi, T.; Yamazaki, I.; Nishimura, Y.; Ohno, T.; Nozaki, K. *J. Am. Chem. Soc.* **1993**, *115*, 4577.

(44) The CR rates in donor−acceptor linked dyads are known to increase with increasing solvent polarity,[1−7,16,17] whereas the CR processes in donor−acceptor linked triads are subject to the reverse trend.[43] The latter case has been ascribed to a superexchange mechanism, in which CR takes place supposedly via the intermediate charge-separated state. However, both trends were seen in the CR processes of **Fc-ZnP-C$_{60}$**/**Fc-H$_2$P-C$_{60}$** (normal region) and **ZnP-H$_2$P-C$_{60}$** (inverted region), despite the fact that the energy difference between the final charge-separated state and the intermediate state in **ZnP-H$_2$P-C$_{60}$** is smaller than that in **Fc-ZnP-C$_{60}$**/**Fc-H$_2$P-C$_{60}$**. Thus, the superexchange mechanism can be ruled out in the present case.

(45) (a) Winkler, J. R.; Gray, H. B. *Chem. Rev.* **1992**, *92*, 369. (b) McLendon, G. *Acc. Chem. Res.* **1988**, *21*, 160.

Table 6. Lifetime (τ_{CR}) and Rate Constants (k_{ET}) for Charge Recombination in Fullerene-Based Dyad and Triads

	THF ($\epsilon_s = 7.58$)		benzonitrile ($\epsilon_s = 25.2$)		DMF ($\epsilon_s = 36.7$)	
compds	$\tau_{CR}/\mu s$	k_{ET}/s^{-1}	$\tau_{CR}/\mu s$	k_{ET}/s^{-1}	$\tau_{CR}/\mu s$	k_{ET}/s^{-1}
ZnP$^{\bullet+}$-C$_{60}^{\bullet-}$	2.7	3.7×10^5	0.78[a]	1.3×10^6	0.57	1.8×10^6
Fc$^{\bullet+}$-ZnP-C$_{60}^{\bullet-}$	3.7[b]	2.7×10^5	7.5[b]	1.3×10^5	16[b]	6.3×10^4
Fc$^{\bullet+}$-H$_2$P-C$_{60}^{\bullet-}$	*c*	*c*	8.3	1.2×10^5	19	5.3×10^4
ZnP$^{\bullet+}$-H$_2$P-C$_{60}^{\bullet-}$	34	2.9×10^4	21[a]	4.8×10^4	20	5.0×10^4

[a] From ref 21. [b] From ref 18. [c] Not determined.

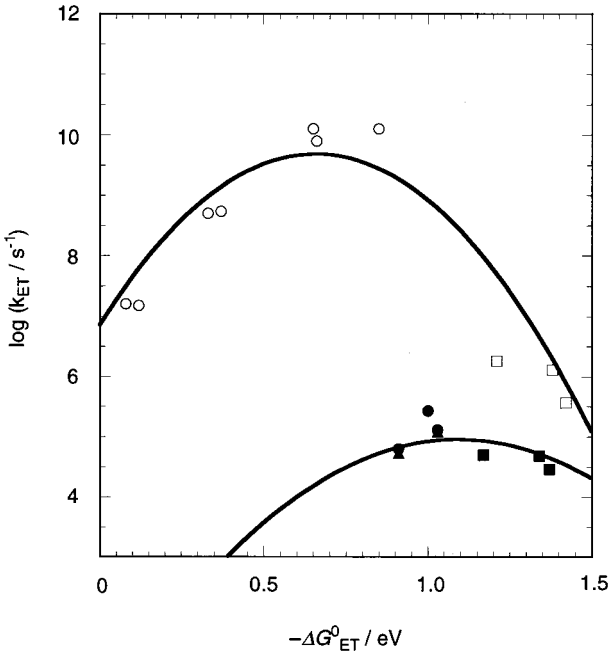

Figure 5. Driving force ($-\Delta G^0_{ET}$) dependence of intramolecular ET rate constants in **ZnP-C$_{60}$** (CS, open circle; CR: open square), **Fc-ZnP-C$_{60}$** (CR, solid circle), **Fc-H$_2$P-C$_{60}$** (CR, solid triangle), and **ZnP-H$_2$P-C$_{60}$** (CR, solid square). The curves represent the best fit to eq 3 (**ZnP-C$_{60}$**: $\lambda = 0.66$ eV, $V = 3.9$ cm^{-1}; **Fc-H$_2$P-C$_{60}$**, **Fc-ZnP-C$_{60}$**, and **ZnP-H$_2$P-C$_{60}$**: $\lambda = 1.09$ eV, $V = 0.019$ cm^{-1}).

processes from the singlet and triplet excited states of the C_{60}, the singlet excited state of the porphyrin, and the CR processes are located in the normal, top, and inverted regions of the Marcus parabola, respectively.[48] The reorganization energy (λ) in **ZnP-C$_{60}$** (0.66 eV) is smaller than those reported previously for porphyrin−quinone[16] and zincporphyrin−freebase porphyrin[17] linked dyads, which typically are in the range between 0.8 and 1.2 eV. This comparison supports our earlier hypothesis that the reorganization energy of fullerenes in ET is indeed exceptionally low.[6−8]

On the other hand, for the triad systems (i.e., **Fc-ZnP-C$_{60}$**/**Fc-H$_2$P-C$_{60}$**/**ZnP-H$_2$P-C$_{60}$**) the following values were extracted: $\lambda = 1.09$ eV and $V = 0.019$ cm^{-1}. Consequently, the λ value in the **ZnP-C$_{60}$** dyad is 0.43 eV smaller than that of the **Fc-ZnP-C$_{60}$**, **Fc-H$_2$P-C$_{60}$**, and **ZnP-H$_2$P-C$_{60}$** triads.[49] Such a difference in λ values between molecular dyads and triads is consistent with the Marcus theory,[9] which predicts an increase of reorganization energy (0.37 eV) with an increase in the donor−acceptor distance from 11.9 Å for the dyad to 30.3 Å for the triads.[50] Thus, the λ values in the present systems are sensitive to the distance where the λ values are rather insensitive to the solvent polarity (THF, benzonitrile, and DMF) at the fixed distance.[46,49] Interestingly, the λ value of the triad systems (1.09 eV) is located between the driving force of the CR process in the **Fc$^+$-ZnP-C$_{60}^{\bullet-}$**/**Fc$^+$-H$_2$P-C$_{60}^{\bullet-}$** (normal region) and **ZnP$^{\bullet+}$-H$_2$P-C$_{60}^{\bullet-}$** pairs (inverted region). This, in turn, provides a reasonable explanation for the opposite dependence of the lifetimes on the solvent polarity between the two systems (vide supra).

It should be noted here that the *V*-value in **Fc-ZnP-C$_{60}$**, **Fc-H$_2$P-C$_{60}$**, and **ZnP-H$_2$P-C$_{60}$** ($V = 0.019$ cm^{-1}) is quite small, as compared to those in **ZnP-C$_{60}$** ($V = 3.9$ cm^{-1}) as well as conventional dyads (∼1−100 cm^{-1}).[1−6,16,17] The distance dependence of electronic couplings, *V*, is frequently described by eq 4:

$$V^2 = V_0^2 \exp(-\beta_{CR} R_{ee}) \qquad (4)$$

where V_0 is a maximal electronic coupling and β_{CR} is a decay coefficient (damping factor) that depends primarily on the nature of the bridge molecule. The β_{CR} value is calculated to be 0.58 Å^{-1}, which is within a boundary of nonadiabatic ET reactions for saturated hydrocarbon bridges (0.8−1.0 Å^{-1}) and unsaturated phenylene bridges (0.4 Å^{-1}).[51]

Conclusion

In summary, highly efficient photosynthetic ET has been realized in a porphyrin−fullerene linked system, i.e., ferrocene−zincporphyrin−C_{60} triad, in which the long-lived charge-separated state (up to 16 μs) can be produced with an extremely

(46) Recently Osuka et al. reported 1,4-phenylene-bridged zincporphyrin−freebase porphyrin dyads with similar reorganization energies in THF ($\lambda = 0.82$ eV) and DMF ($\lambda = 0.84$ eV) despite the large difference in the solvent polarity.[17b] This was rationalized in terms of the small reorganization energies of porphyrins leading to a delocalization of the positive and negative charges. The delocalization in C_{60}, provided by its large three-dimensional π system, suggests that the reorganization energy in the present systems is not susceptible to changes in the solvent polarity (i.e., THF, benzonitrile, and DMF). Accordingly, reorganization energies of the dyad and triads are reasonably assumed to be similar in THF, benzonitrile, and DMF.

(47) The semiclassical Marcus treatment including contribution of the nuclear tunneling could not be applied to the present systems, since such analysis made the fitting worse, as compared to the present analysis.

(48) The best fits of eq 3 for **ZnP-C$_{60}$** suffers from the fact that it encompasses data for CS from different excited states and CR to the ground state, i.e., ET rates for different reactions which take place between different electronic states. Excitation and redox experiments with C_{60} indicate that the nuclear coordinates of the fullerene singlet ground, singlet excited, and reduced states are similar. Since porphyrins and fullerenes have small reorganization energies and the Coulombic interaction in **ZnP$^{\bullet+}$-C$_{60}^{\bullet-}$** ($R_{ee} = 11.3$ Å)[21] is negligible, the electronic coupling as well as the intramolecular reorganization energies may be similar. This justifies plotting the CS and CR rates on the same curve.

(49) Considering the similarity in the intervening spacers between the ferrocene and the C_{60} in **Fc-H$_2$P-C$_{60}$** and **Fc-ZnP-C$_{60}$** and the zincporphyrin and the C_{60} in **ZnP-H$_2$P-C$_{60}$**, the *V* values in the two systems may well be identical. Since a charge of ferrocene is protected from solvation due to the bulky cyclopentadienyl rings, both the triads are assumed to give similar small λ values. This is consistent with the fact that ferrocenes are frequently employed as an internal standard in electrochemical measurements. Porphyrins are also known to exhibit small λ values; see: Fukuzumi, S. In *The Porphyrin Handbook*; Kadish, K. M., Smith, K. M., Guilard, R., Eds.; Academic Press: San Diego, CA, 2000; Vol. 8, pp 115−151.

(50) The difference in the λ values ($\Delta\lambda = 0.37$ eV) is estimated from the following equation: $\Delta\lambda \approx (\epsilon^2/n^2)[(1/R_{ee}(\text{dyad})) - (1/R_{ee}(\text{triad}))] = 7.2 \times [(1/(11.9)) - (1/(30.3))]$.[9]

(51) Helms, A.; Heiler, D.; McLendon, G. *J. Am. Chem. Soc.* **1992**, *114*, 6227.

high quantum yield (nearly unity). This can be rationalized by the small reorganization energy of C_{60} in multistep ET processes, where forward ET is accelerated and back ET is decelerated. It should be noted here that both the normal and inverted regions of the Marcus parabola have been observed for intramolecular CR processes in the covalently linked triads. In addition, we have successfully shown the dependence of the ET rate constants on both the distance and driving force in a series of homologous porphyrin−fullerene linked systems. The fundamental information on ET obtained here will be helpful for the design of artificial photosynthetic systems.

Acknowledgment. This work was supported by Grant-in-Aids for COE Research and Scientific Research on Priority Area of Electrochemistry of Ordered Interfaces and Creation of Delocalized Electronic Systems from the Ministry of Education, Science, Sports and Culture, Japan, a Millennium Project from the Science and Technology Agency, Japan (No. 12310), and the Office of Basic Energy Sciences of the Department of Energy, USA. H.I. thanks the Sumitomo Foundation for financial support. This is document NDRL-4260 from the Notre Dame Radiation Laboratory.

Supporting Information Available: Experimental details including synthetic procedures and characterization (pp S1−S7), mathematical derivations for ET rate constants and formation efficiencies of each state (pp S8−S9), differential pulse voltammograms of **ZnP-NHCO-ref** in THF, benzonitrile, and DMF (p S10), and nanosecond transient absorption spectra of **Fc-ZnP-C_{60}** (p S11) and **Fc-H_2P−C_{60}** (p S12) in benzonitrile (PDF). This material is available free of charge via the Internet at http://pubs.acs.org.

JA003346I